

UTILIZATION OF SATELLITE AND RADAR DATA IN SHORT RANGE PREDICTION MODELS

Department of Meteorology
University of Wisconsin—Madison
1225 W. Dayton Street
Madison, Wisconsin 53706



Contributions by

C.-B. Chang	V. E. Suomi
D. D. Houghton	R. D. Thomas, Jr.
D. K. Lee	T. A. Wilson
G. F. Sill	

D. D. Houghton, Principal Investigator

FINAL TECHNICAL REPORT

NSF Research Grant ATM77-20231
December 15, 1977 to November 30, 1980
Submitted February 12, 1981

UTILIZATION OF SATELLITE AND

RADAR DATA IN

SHORT RANGE PREDICTION MODELS

Department of Meteorology
University of Wisconsin-Madison
1225 W. Dayton Street
Madison, Wisconsin 53706

Contributions by

C.-B. Chang	V.E. Suomi
D.D. Houghton	R.D. Thomas Jr.
D.K. Lee	T.A. Wilson
G.F. Sill	

D. D. Houghton, Principal Investigator

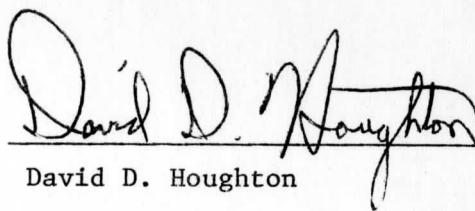
FINAL TECHNICAL REPORT

NSF Research Grant ATM77-20231
December 15, 1977 to November 30, 1980

Submitted February 12, 1981

This Report is submitted to satisfy the
National Science Foundation requirements
of a Final Technical Report
for Grant ATM77-20231.

Principal Investigator



David D. Houghton

February 12, 1981

TABLE OF CONTENTS

I.	Introduction	1
II.	Scientific Description of Project and Results	1
	A. Production and Quality Analysis of Mesoscale Data Sets	
	B. Objective Analysis Procedures	
	C. Data Insertion Techniques	
	D. Impact on Model Simulation	
	E. Improvement in Model Forecasts	
III.	Publications	9
	A. Journal Papers	
	B. Conference Preprints and Reports	
IV.	Student Degrees	9
	A. Listing	
	B. Abstracts of Theses	
V.	Miscellaneous	12
	A. Papers Presented at Meetings (not listed in III-B)	
	B. Other students supported	
VI.	Copies of Publications	13

I. INTRODUCTION

This report provides a technical summary of the work and students supported by research grant ATM77-20231. Sections II, III and IV give an overview of the scientific accomplishments. A detailed scientific discussion is presented in the published papers, conference preprints, and theses which resulted from the research. Copies of these, except for the theses, are included in Section VI.

II. SCIENTIFIC DESCRIPTION OF PROJECT AND RESULTS

This research project continued the mesoscale studies begun in 1975 under NSF Grant ATM75-03617. The research was guided by the acknowledgment that the utilization of many mesoscale data forms in numerical models required considering all of the steps from production of the data through evaluation of the improvement in model simulations resulting from use of this data.

The complexities of data production and the relevant models needed for testing made it not possible to consider many case studies. In fact, only one data set was carried through the entire utilization test procedure in an experiment that provided optimism for further work. The emphasis in the work was on the production and analysis of the basic mesoscale data.

It is evident that much additional work will be required before any conclusions about the utility of current and anticipated mesoscale observations for numerical simulation models can be made. Furthermore, it will be necessary to consider more comprehensive mesoscale descriptions derived from a variety of sources and variables rather than a single variable from a single source such as satellite cloud-derived winds.

In order to provide proper perspective on the results, the scientific summary here considers separately the five steps involved in evaluating the utility of the data.

A. Production and quality analysis of mesoscale data sets

1. Satellite cloud winds

Most of the effort has been with satellite wind information obtained from geosynchronous meteorological satellite data processed on the computer system McIDAS in the Space Science and Engineering Center.

Three data sets were produced for times near 1800 GMT on October 30, 1974, May 6, 1975 and May 20, 1977. Basic characteristics for each were presented by Wilson and Houghton (1979); Lee (1978); and Houghton, Lee and Chang (1979) respectively. The area covered in each was approximately 600 km square in the Midwest region with the lower level (approximately 900 to 700 mb) having better coverage. In some instances, the number of wind vectors obtained at high levels (400 mb and above) was too small to provide a useful horizontal field. In the first two cases the three dimensional coverage was sufficient for an estimate of vertical motion to be attempted by the kinematic method. Resolution was sufficient for features with horizontal length scale as little as 25 km at lower levels, but for derived parameters such as vertical motion which required high level as well as low level information resolution was adequate only to 50 or 75 km. (Note: length scale here is taken to be one quarter of a wavelength.)

Quality of the observations was assessed by comparison of the information with rawinsonde observations and included new estimates of the expected correspondence of cloud-top displacement vectors with rawinsonde observations at the same level. An overall root mean square (RMS) vector difference magnitude of 4.7 m s^{-1} was estimated (Wilson and Houghton, 1979) for middle-latitude baroclinic zone mesoscale wind vectors. Lee (1978) found a RMS difference for u and v components ranging from 2 to 6 m s^{-1} by a detailed comparison of satellite cloud winds within a 1° radius of the rawinsonde station to the rawinsonde data. The difference of the mean of the satellite wind data from the rawinsonde values was generally less than 3 m s^{-1} at middle and low levels demonstrating a

correspondence that could be obtained by averaging cloud wind data. The comparison study for the May 20, 1977 data had the advantage of a special 1800 GMT rawinsonde observations eliminating errors introduced by time interpolation. Results showed slightly better correspondence between the two data forms (Ph.D. thesis work of D.K. Lee). These studies suggested that the noise level produced by mixing satellite and rawinsonde information would not be larger than the variance in each data type separately. Furthermore the expected noise level in mesoscale divergence and vorticity was shown to be roughly half of typical magnitudes of these quantities.

The features of divergence, vorticity and vertical motion determined from the first two data sets corresponded well to synoptic phenomena. In the first case, the computed vertical motion pattern was consistent with the subsequent outbreak of severe convective weather events. In the second case, realistic correspondence to frontal activity and convective structure (or the lack of such) was noted. The third data set is being enlarged and examined further by Lee in continuing Ph.D. thesis work.

These studies have provided confidence that mesoscale wind information obtained from satellite cloud imagery will be able to contribute to general mesoscale description and will have horizontal resolution of well-averaged data at low levels equal to or better than the surface hourly reporting station network over the United States.

2. Satellite temperature sounding data

In conjunction with the VAS experiment work being conducted at the University of Wisconsin by the National Environmental Satellite Service (NESS/NOAA), mesoscale temperature sounding data for the Midwest United States (SESAME area) has been produced for April 10, 1979 using TIROS-N data. The effective horizontal resolution obtained corresponds to a length scale of 60 km or the resolution obtained from a network with twice the mean station separation

of the existing surface hourly reporting network.

This data will be carried through the five steps of the utilization-test procedure by M. Kalb in Ph.D. research just initiated.

3. Radar precipitation data

Two studies were made with radar data to assess the potential for using such information as an explicit parameter for the initialization and output of deterministic prediction models.

An earlier extensive statistical analysis performed on Midwestern United States radar data (Mielke and Houghton, 1977, J. Appl. Meteor., 16, 833-843) showed that precipitation in warm frontal regions did have a scale of organization that was sufficient for carrying it as an explicit prediction parameter in a short-range regional mesoscale prediction model. In particular, time scales (lifetimes) were in the 4-12 hr range and the typical half width scale in space was 75 km. Precipitation systems associated with cold fronts had smaller scales for the group structure, namely 3-8 hr for lifetime and 55 km for half width. These would still be sufficient for meaningful explicit representation in a mesoscale model. The air-mass convective precipitation systems had a 3-5 hr scale for lifetime and typical half width of 30 km and thus are in the marginal range for explicit simulation.

The first study (Thomas Jr., and Houghton, 1979) focused on correlations between radar echo characteristics and other meteorological parameters such as upper level and surface wind characteristics in the vicinity of cold fronts. This was pursued with the hope that simple prediction models could be formulated. This goal was never achieved. Nevertheless, the relationships between some features of the surface data and radar echos should be useful in the process of combining surface weather observations with information at higher levels.

The second study (Sill, 1981) examined the properties of the precipitation areas in the warm frontal zone for the vigorous April 3-4, 1974 storm in

the Midwest United States. Here the focus was more on the relationship to upper air parameters including vertical wind shear and static stability. General agreement with existing theories for warm front rain bands was noted. Verifying such theoretical models provides optimism for formulating short range prediction models.

4. Satellite cloud and water vapor data

A brief analysis of the European METEOSAT images for February 2, 1978 was made because of interest in the new possibilities for atmospheric description (including the mesoscale) from water vapor channel data (Houghton and Suomi, 1978).

B. Objective analysis procedures

From the very start, it was recognized that objective analysis would be an important factor for handling mesoscale data. It was clear that the heterogeneous nature of the observations, the inhomogeneity in spatial and time coverage, and the lack of simple relationships and conceptual models for mesoscale phenomena would make the development and study of objective analysis procedures important.

Early work (Wilson and Houghton, 1979) adopted a scheme developed at the Stanford Research Institute by Mancuso and Endlich which represented a method originally designed for synoptic scale studies. Variations in the parameter specifications for this approach were studied by Lee (1978). Attention has been given to the performance of more recently considered techniques for mesoscale meteorology on the satellite cloud wind data sets (Houghton, Lee and Chang, 1979). In particular methods developed by Barnes and Gardin were examined. It was found that the magnitude differences between methods for divergence and vorticity values were nearly equal to the magnitudes themselves on a 35 km grid. Obviously the objective analysis procedure will remain an important factor.

C. Data insertion techniques

Little was done in this research program to experiment with actual initialization procedures. The first simulation test with a comprehensive mesoscale model used a simple single-time direct replacement for velocity without altering the mass or moisture field (Houghton, Lee and Chang, 1979). It was understood that this represented a baseline as the most unsophisticated approach. Later experiments in the Ph.D. work of Lee have tested velocity insertion gradually imposed over a 30 min time period. Results showed large spurious pressure oscillations not found with the simple single-time imposed insertion test.

D. Impact on model simulation

Analysis of the model output in the assimilation tests with the May 20, 1977 satellite wind data (Houghton, Lee and Chang, 1979 and subsequent Ph.D. research of Lee) has documented some of the impacts of the inserted satellite wind data. The vorticity patterns in the satellite wind data tended to be persistent over the entire 6 hour period of the forecast. On the other hand, horizontal divergence fields changed rapidly during the first hour of the forecasts and it was difficult to identify a meaningful signature in this parameter distinct from the control case fields after 3 hours.

The general effect of the input satellite wind information is in the modification of amplitudes of mesoscale features that develop in the control forecast rather than the introduction of alternate features.

Analysis of difference maps and time series at individual grid point time series data showed a variety of "noise" components induced by the data insertion. Gravity waves propagated outward from the insertion area at roughly 30 m s^{-1} showing highest amplitudes along the flow lines in the upper troposphere through this area. The amplitudes of the $2 \Delta t$ oscillations were very

small. Oscillations with periods of 15 minutes and the order of $1\frac{1}{2}$ hours were also noted.

Analysis of the model impacts of this new mesoscale information is just in the preliminary stage and will be an important component of subsequent research work.

Studies have been made concerning basic concepts of adjustment theory and dynamics of subsynoptic scale motions which should be of some assistance for diagnosing the response of comprehensive numerical models to mesoscale data insertion. An analysis of prognostic and diagnostic methods for isolating the non-quasigeostrophic (gravity-inertial) motions in a simple two-layer simulation of the atmosphere were made using the primitive equations [Houghton, Campbell and Reynolds (1979, unpublished manuscript)]. Results showed a coherent pattern in the gravity-inertial motion component that remained in the vicinity of a jet stream maximum. Another study underway by Hyde for Ph.D. research work is focusing on analytical and simple numerical solutions for the interactions between a synoptic-scale jet flow and co-existent gravity-inertial modes.

E. Improvement in model forecasts

This has been a very difficult area for study due to the lack of three dimensional mesoscale observations for verification purposes.

A very crude comparison of satellite wind fields with model simulations (6 hr forecast) verifying at observation time was made by Lee (1978) for the May 6, 1975 data set in order to test the overall compatibility between the two elements. Unfortunately the model (Drexel-NCAR Regional Mesoscale Model) had a horizontal grid spacing of 70 km and thus could not represent the 25 km length scales in the observations. Nevertheless, there was some correspondence in the u and v velocity component fields and even in the divergence and vorticity patterns. Lee (1978) went on to determine statistics for the model

verification in terms of rawinsonde and the satellite wind data. In general the model data differed more from either the rawinsonde data or the satellite winds than the latter two differed from each other.

A determination of the actual improvement in model forecasts was attempted for the test insertion of satellite cloud winds into the Drexel-NCAR mesoscale model described by Houghton, Lee and Chang (1979). The only verification parameter available was for precipitation from the National Weather Service radar observations. The model control case 6 h forecast corresponded well with the observations for a squall line in western Oklahoma and North Central Texas and a diminishing squall line in Wisconsin and Texas. The satellite wind insertion case showed an improvement in the forecast over Illinois and to the south and over Missouri. Nevertheless, no meaningful conclusion on forecast improvement could be made.

III. PUBLICATIONS

A. Journal Papers

Houghton, D.D. and V.E. Suomi, 1978: The information content of satellite images. Bull. Amer. Met. Soc. 50, 1614-1617.

Thomas, Jr., R.D. and D.D. Houghton, 1979: The relationship between cold frontal radar echoes and selected surface kinematic parameters. Mon. Wea. Rev., 107, 1589-1599.

Wilson, T.A. and D.D. Houghton, 1979: Mesoscale wind fields for a severe storm situation determined from SMS cloud observations. Mon. Wea. Rev., 107, 1198-1209.

B. Conference Preprints and Reports

Houghton, D.D., D.K. Lee and C.B. Chang, 1979: Numerical Model Initialization with Subsynchronous-Scale Satellite Cloud-Wind Data. Fourth AMS Conference on Numerical Weather Prediction. October 29 - November 1, Silver Spring, Maryland. Preprint Volume. pp. 16-23.

IV. STUDENT DEGREES

A. Listing

Lee, Dong K., 1978: Characteristics of middle-latitude subsynoptic scale winds from satellite observations: a case study. M.S. Thesis, 94 pp.

Thomas, Jr., Richard D., 1978: The relationship between cold-frontal radar echoes and selected surface and upper air parameters. M.S. Thesis, 119 pp.

Sill, Gordon F., 1981: Rainbands ahead of a warm front: A case study. M.S. Thesis (in press).

B. Abstracts of Theses

Lee, Dong K., 1978: Characteristics of middle-latitude subsynoptic scale winds from satellite observations: a case study. M.S. Thesis, 94 pp.

ABSTRACT

Subsynoptic scale cloud winds are obtained from SMS-1 images in the mid-latitude baroclinic region for the Omaha tornado case of 6 May 1975. Kinematic fields are computed from the cloud wind data using the SRI objective analysis scheme and their correspondence to the synoptic situations is discussed. Some statistical comparisons between the cloud and rawinsonde wind data are made in terms of root mean square differences. In order to investigate the possibility of using cloud wind data to initialize numerical models, the cloud wind data are compared directly to regional scale mesoscale numerical model outputs.

The kinematic fields computed from the cloud wind data are generally consistent with the synoptic phenomena ahead of the cold front. The magnitudes of divergence and relative vorticity are the order of 10^{-4} sec^{-1} for this study. The differences of the cloud winds from the rawinsonde winds are no larger than rawinsonde data errors themselves. In the comparison between the cloud wind and numerical model outputs there is good correspondence for the v component winds and relative vorticity and general qualitative agreement of vertical velocity patterns.

Thomas Jr., Richard D., 1978: The relationship between cold-frontal radar echoes and selected surface and upper air parameters. M.S. Thesis, 119 pp.

ABSTRACT

This study examines the relationship between the radar echo parameters of motion, area coverage and intensity, and the upper level winds, surface divergence, surface divergence of moisture flux and surface relative vorticity in cold front situations. Good correlations were found between echo motion and upper level winds. The relationship between the other radar echo parameters and the surface kinematic parameters were not as good, but gave some positive results. The best correlations were between echo intensity and relative vorticity. The correlations were improved by using surface data one hour before the time of the echo. The study used fine resolution digitized radar data which was analyzed on a computer-interactive video system.

Sill, Gordon F., 1981: Rainbands ahead of a warm front: A case study.

M.S. Thesis (in press).

ABSTRACT

A case study of mesoscale precipitation areas (rainbands) was performed for a storm which passed through the Midwest on 3 and 4 April, 1974. Tracings from the PPI scope of seven radars were correlated to obtain an entire radar picture of each rainband's movement. Twenty-six rainbands were studied with respect to the wind, temperature, and moisture fields of the storm. The average rainband length was 386 km, the average width 38 km, and the average length-to-width ratio was 29:1. The average duration of a rainband was about 5 hours.

The rainbands occurred in two "belts" one south and one north of the warm front. The rainbands would develop and grow at the southern end of the belt, travel to the northern end and stop. At the beginning of the storm the rainbands would dissipate when they reached the northern end of the belt, but as the storm progressed they did not dissipate, but rather began to "stack up" as each successively reached that end. Eventually, this produced a wide, stationary area of precipitation within each belt about 95 - 140 km wide and 185-650 km long. Thus the entire area north and south of the warm front became covered by a large stationary area of precipitation as is commonly associated with warm fronts as seen on radar.

The cloud layer in which the rainbands developed was between 14,000 and 16,000 feet msl. A potentially unstable layer was associated with the cloud layer and it is assumed that the rainbands were caused by the release of this instability as the air rose over the warm front. The greater majority of the rainbands moved to the left of the wind in the cloud layer. They did not move perpendicular to their orientation, but averaged 46° to it. The rainbands were approximately parallel to the warm front and were found to be approximately parallel with the shear vector in the cloud layer in accord with Asai's (1972) theory. About 50% of the rainbands had significant changes in their orientation as they travelled north, most rotating counterclockwise. A rainband signature in the surface pressure field was looked for, but not found.

The rainbands were found to have a systematic evolution, organization, and movement. The results were in agreement with the results and theories of other researchers throughout the world. This points to the general applicability of the results to cyclonic storms.

V. MISCELLANEOUS

A. Papers Presented (not listed in III-B)

Houghton, D.D., 1978: "Mesoscale analysis studies". Limited Area and Mesoscale Prediction System (LAMPS) Workshop, May 3, NCAR, Boulder, Colorado.

B. Other Students Supported

Hyde, Richard (Sandy)

Kalb, Michael

Slye, Barbara

VI. COPIES OF PUBLICATIONS

These are presented in the same order as listed in Section III.

Information Content of Satellite Images

David D. Houghton and Verner E. Suomi, *Department of Meteorology and Space Science and Engineering Center, University of Wisconsin, Madison, Wis. 53706*

Abstract

The correspondence of structures noted in the Meteosat water vapor channel images to conventional tropical streamline analyses for 8 February 1978 is presented. Results demonstrate the dramatic new possibilities available with the water vapor channel data.

Views of the earth's clouds taken from polar-orbiting satellites have been with us since 1960, almost two decades, and images from geostationary satellites have been available since 1966, more than one decade. One has a strong intuitive impression that the classical weather map and the satellite image should be more directly related to each other in a quantitative sense than they appear to be. Attempts to obtain temperature and moisture soundings from polar-orbiting satellites have not yet made a profound impact on the quantitative description of the atmosphere in the Northern Hemi-

sphere already obtained from a wide source of data. On the other hand, the satellite has already made an improvement in the atmospheric description of the Southern Hemisphere, where the conventional data coverage is extremely deficient.

The problem of relating satellite data with conventional atmospheric data was recently made more dramatic to us as a result of a small wager. One of us (V.E.S.) had the good fortune to visit the European Space Operations Center at Darmstadt, F.R.G., and thanks to John Morgan was provided with three sets of visible, IR, and water vapor images taken from the new European geostationary satellite, Meteosat. A remarkable feature of the new water vapor images ($5.7\text{--}7.1\ \mu\text{m}$ channel data) is that they allow dramatic views of global-scale as well as synoptic-scale entities with definite structures (Morel *et al.*, 1978). Some of the possible applications arising from the more continuous nature and clear air coverage of the water vapor images in contrast to cloud data have been discussed by Allison *et al.* (1972), Steranka *et al.* (1973), Rodgers *et al.* (1976), and most recently by Morel *et al.* (1978). The first three studies considered the orbiting Nimbus satellite data, and the last outlined possibilities offered by geosynchronous satellites such as Meteosat.

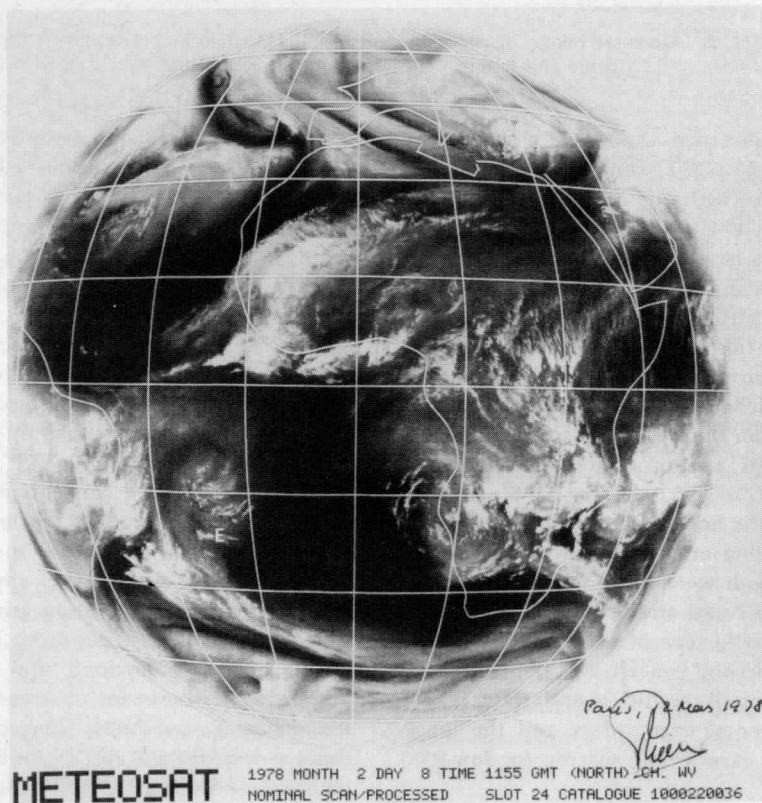


FIG. 1. Meteosat image in the water vapor channel ($5.7\text{--}7.1\ \mu\text{m}$), 1155 GMT, 8 February 1978. Latitude and longitude lines are shown at 15° intervals. The symbol E denotes the region where air flow "appears" to be easterly.

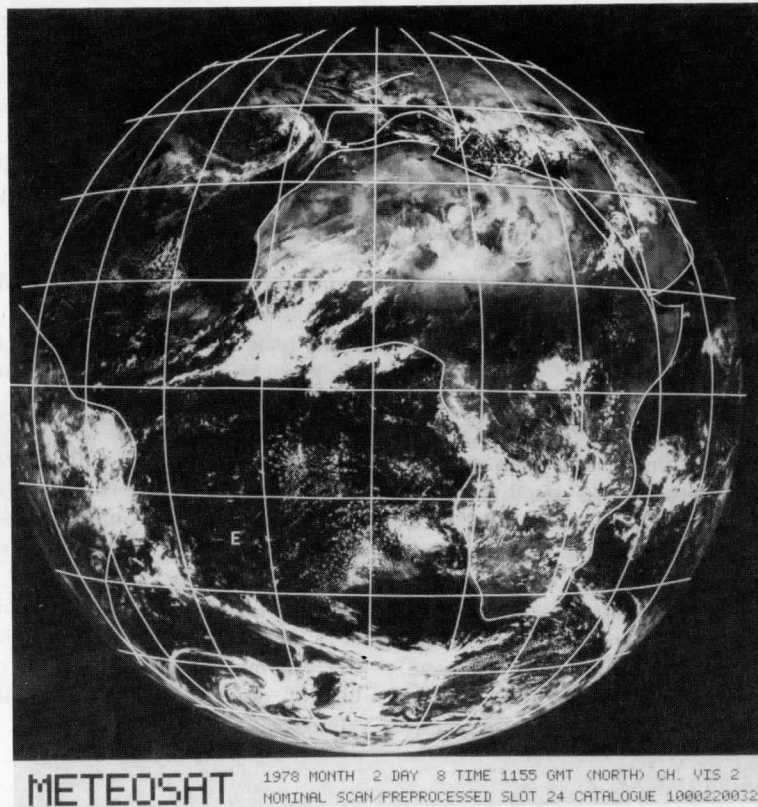


FIG. 2. Meteosat image in the visible channel, 1155 GMT, 8 February 1978. Latitude and longitude lines are shown at 15° intervals.

The case debated concerned the water vapor image for 8 February 1978, 1155 GMT, which is shown in Fig. 1. One sees a vortex pair, with one center at 15°S, 25°W and the other at 20°S, 12°E (some 3500 km apart), that in the image appears to have a strong northerly current between the centers. Actually, one sees many of these vortex pairs on a wide variety of scales from the smallest to the largest in all of the water vapor channel images. They are an easily seen and very dominant structure. The image in the visible channel for the same time (Fig. 2) shows little signal from the western part of this vortex pair and fails to reveal any pronounced structure or symmetry for it.

The wager was over the notion that one of the vortices was cyclonic and the other anticyclonic, whereas the opposing view was that both were cyclonic. The argument for the first concept was based on the clear impression of a vortex pair with a single type of weather in between. The argument for the second concept was the concentration of similarly organized cloudiness and water vapor maximums at the center of each vortex and the longitudinal spacing, which exceeds the spacing for low-level tropical disturbances.

Resolving the issue required obtaining conventional data for the same date that would correspond to the satellite image. Since the data showed the clouds near the vortices to be in the upper troposphere, and since the water vapor channel data is most sensitive to condi-

tions in the 250–550 mb layer (with maximum response near 400 mb), this required examining upper tropospheric wind analyses for a subtropical area that has minimal rawinsonde data. The National Meteorological Center Mercator projection tropical streamline charts for 250 and 500 mb for the time period 1200 GMT, 7 February 1978, to 1200 GMT, 9 February 1978, were used. The time sequence allowed for determination of time continuity of the analyzed features (essential in this area of minimal data) and determination of propagation rates so that trajectory-streamline relationships could be discussed.

Figure 3 shows the conventional data at 250 and 500 mb for the same time as the satellite pictures in Figs. 1 and 2. Regions with wind speeds <10 kt (5 m/s) are specially noted since these appear to correspond to centers of circulation. (Propagation speeds of the systems were very small, ranging from 0 to 10 kt (5 m/s) eastward.) Centers of cyclonic and anticyclonic circulation and center positions for the two vortices observed in the satellite image are shown. The conventional 250 mb data show a deep trough and cyclonic center at 25°W, 15°S, with a broader but weaker anticyclonic circulation centered near 15°E, 15°S. The 500 mb data show the same features, although both are slightly weaker and the anticyclonic circulation centers are located around and not at 15°E, 15°S. Not only is the fit good, but it must also be called a direct bull's-eye hit. The fit is exact.

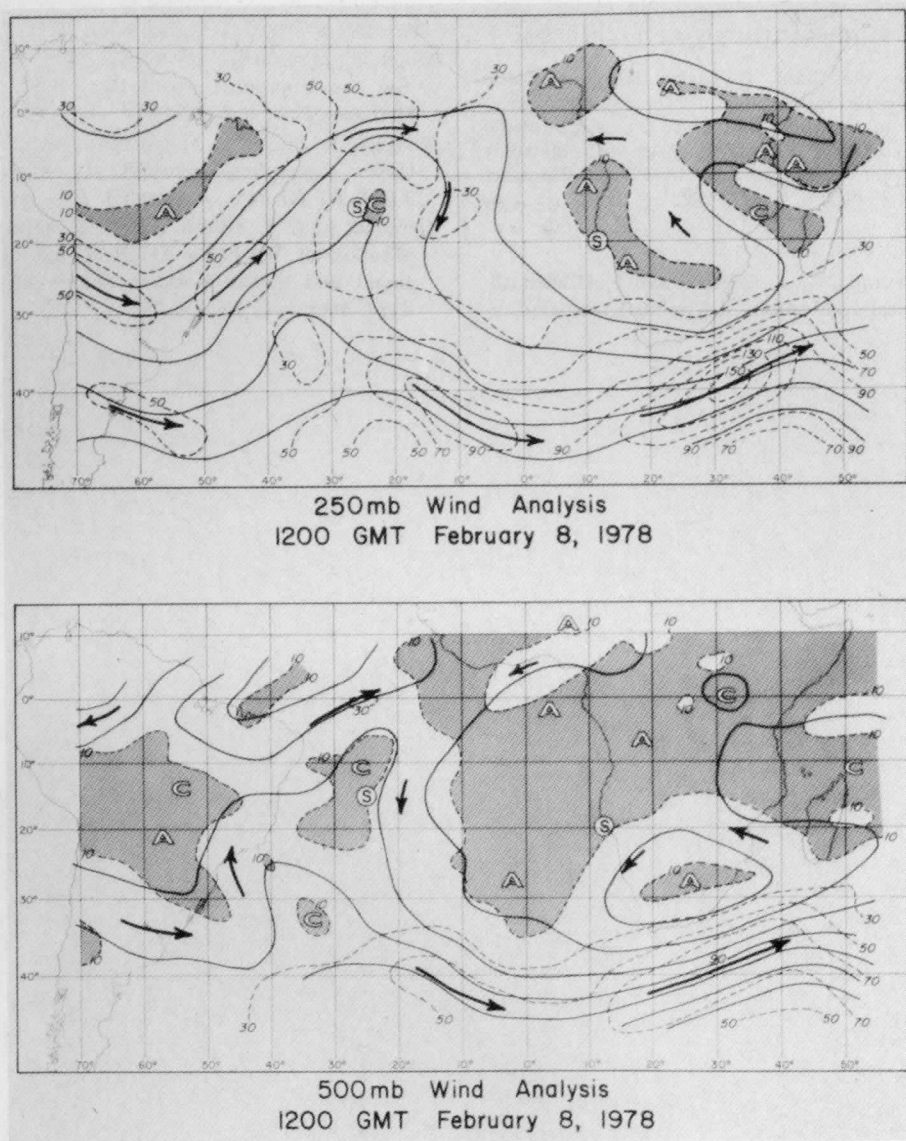


FIG. 3. Tropical streamline charts for 1200 GMT, 8 February 1978, at 250 and 500 mb. Solid lines are streamlines and dashed lines are isotachs labeled in knots. Shaded areas denote regions where wind speed is < 10 kt (5 m/s). Arrows show wind flow at local speed maximums. The symbols C and A mark centers of cyclonic and anticyclonic circulation, respectively. The two centers of the vortex pair observed in the satellite water vapor image and discussed in this paper are shown by the letter S. Data were taken from National Meteorological Center Mercator projection charts.

Who won the wager is not important, but what is important is the fact that in the image the anticyclone is organized as strongly as the cyclone, a fact that one would never deduce from the conventional data, even though the data density for the two regions is about the same. The circulation strength in the cyclonic system implies a period of roughly 4 days for air to make one revolution about the center. The period is more than double for the anticyclonic region and would appear to exceed the time scale of coherency expected for the system. Furthermore, in the region marked E in Fig. 1 ($\sim 25^\circ$ W, 25° S), one would have guessed easterly winds

to exist. Yet at that spot we find weak northwesterlies in the conventional data. It thus appears that much of the organization is *relative to the entity*, and this high degree of organization is lost (except with exceedingly accurate observations) using Eulerian observations.

Demands for obtaining more relevant and useful information from satellites will certainly increase because of advancing expectations in mesoscale meteorology and the needs for large-scale analyses such as in the Global Weather Experiment. An important task is to learn how to take better advantage of the organization and struc-

ture revealed only by satellite photographs and to integrate this information quantitatively with other data.

Acknowledgments. We thank Dr. John Morgan of the European Space Operations Center at Darmstadt, F.R.G., and Dr. Pierre Morel at the Laboratoire de Météorologie Dynamique, CNRS, France, for providing us with Meteosat image pictures. Support was provided by NOAA Contract DOC7-35217 and NSF Grant ATM77-20231.

References

Allison, L. J., J. Steranka, G. T. Cherrix, and F. Hileenrath, 1972: Meteorological applications of Nimbus-4 temperature-

humidity infrared radiometer, 6.7 μm channel data. *Bull. Am. Meteorol. Soc.*, **53**, 526-535.

Morel, P., M. Desbois, and G. Szejwach, 1978: A new insight into the troposphere with the water vapor channel of Meteosat. *Bull. Am. Meteorol. Soc.*, **59**, 711-714.

Rodgers, E. B., V. V. Salomonson, and H. L. Kyle, 1976: Upper tropospheric dynamics as reflected in Nimbus-4 THIR 6.7 μm data. *J. Geophys. Res.*, **81**, 5749-5758.

Steranka, J., L. J. Allison, and V. V. Salomonson, 1973: Application of Nimbus-4 THIR 6.7 μm observations to regional and global moisture and wind field analyses. *J. Appl. Meteorol.*, **12**, 386-395. ●

The Relationship between Cold-Frontal Radar Echoes and Selected Surface Kinematic Parameters

RICHARD D. THOMAS, JR.¹

Systems Development Office, National Weather Service, NOAA, Silver Spring, MD 20910

DAVID D. HOUGHTON

Department of Meteorology, University of Wisconsin, Madison 53706

(Manuscript received 1 February 1979, in final form 10 August 1979)

ABSTRACT

This study examines the relationship between the radar echo parameters of area coverage and intensity, and the surface kinematic fields of divergence, divergence of moisture flux and relative vorticity. The study was limited to 11 cold frontal cases during the period March 1976–March 1977, and involved 99 echoes. Fine-resolution digitized radar data were used from two midwestern and one eastern United States sites. The data were analyzed on a computer-interactive video system. The area coverage did not correlate significantly with any of the surface parameters tested. However, the intensity parameters did show significant relationships with the surface parameters, the best being with relative vorticity. The correlations were higher when surface data from 1 h before the time of the echo were used, with coefficients as high as 0.5.

1. Introduction

The forecasting of precipitation always has been an important aspect of operational weather forecasting. In recent years, much work has been done toward producing more accurate and more automated short-range local precipitation forecasts.

A problem in any objective mesoscale forecasting is that of getting observational data on a small enough scale. Surface observing stations are generally ~100 km apart, and upper air observing stations are 300–400 km apart. On the other hand, radar and satellite data are of a continuous nature, in both time and space. The use of radar in precipitation forecasting is the motivation behind this investigation.

In order to use radar as an objective tool in precipitation forecasting, procedures must be developed to forecast echo movement and changes with time. Several extrapolation techniques have been developed which give favorable results (see Elvander, 1976). However, these forecasts probably could be improved by using relationships with other atmospheric variables in addition to the extrapolation techniques. First, however, these relationships must be better understood.

The objective of this analysis was to examine the relationships between radar parameters (such as area coverage, growth, intensity and the change of these parameters in time) and surface kinematic fields [such as divergence, divergence of moisture (mixing ratio) and relative vorticity]. These kinematic fields were expected to have a direct relationship with precipitation. Surface data were preferred over upper air data because of greater abundance in time and space.

Numerous studies in the past have successfully related the echo movement to upper level winds, particularly the 700 mb level (see Harper and Beimers, 1958; Boucher and Wexler, 1961; Newton and Fankhauser, 1964; Cruz, 1973; Mielke and Houghton, 1977). Far less has been done concerning relationships with the surface variables, particularly relationships between subsynoptic-scale data and the detailed features of individual radar echoes. To limit the scope of this study, only cold frontal echoes were used.

2. Past work

Byers and Braham (1949) reported that during the Thunderstorm Project, weak convergence was present during the early cumulus stage of thunderstorm development. This was 20–30 min before the radar detected the storm. However, when older storms were in the area, their outflow dominated the sur-

¹ Research was carried out while author was on a fellowship program at the Department of Meteorology, University of Wisconsin at Madison.

TABLE 1. Characteristics of WSR-57.¹

Wavelength	10.3 cm
Transmitted frequency	1250 MHz
Beam width	2°
Range	125 n mi
Pulse repetition frequency	164 pps
Width of pulse	4 s
Peak transmitted power	410 kW
Scan rate	3 rpm
Antenna gain	38 dB
Standard antenna elevation	0.5°

¹ Information received by personal communication with Jim Schaeffer, Office of Technical Services, National Weather Service, June 1978.

face wind. This made it impossible to find areas of inflow near new storms.

Austin and Blackmer (1956) studied the precipitation patterns of 30 summertime cold fronts in Massachusetts using radar data. Synoptic-scale parameters such as the 700 mb temperature contrast across the front, warm air static stabilities and 850 mb dew-point spread were correlated to the area covered by precipitation. The correlation coefficients were generally poor, ranging from 0.0 to 0.4. In a similar study with wintertime cold-frontal precipitation, Cox (1959) found that out of seven synoptic-scale parameters, only an instability index correlated significantly with total radar-scope coverage. Twenty-one cold-frontal situations were used for that study.

In another study, Myers (1964) studied the role of the synoptic situation and local topography on the pattern of showers in central Pennsylvania. In comparing several synoptic variables with the amount of radar scope coverage, the surface dew-point depression produced the highest significant correlation coefficient. The synoptic parameters were also compared with various "scope scatter" coefficients. Again dew-point depression showed the best relationship.

TABLE 2. Comparison of rainfall rates with radar power returned and D/RADEX levels (by Saffle, 1976). All numbers are range correlated.*

Rainfall rate (mm h ⁻¹)	LogZ	Threshold levels (D/RADEX)
0.508	1.83	1
1.27	2.47	2
2.54	2.93	3
5.08	3.43	4
12.7	4.07	5
25.4	4.55	6
50.8	5.03	7
127.0	5.67	8
254.0	6.15	9

* The D/RADEX rainfall rates were changed after this research was completed (see Saffle and Greene, 1978).

Using data from two experiments carried out in the summers of 1971 and 1973 in southern Florida, Ulanski and Garstang (1978) studied the role of surface divergence and relative vorticity in convective precipitation. Data from a dense observing network, part of the Florida Area Cumulus Experiment, was used to study about 50 storms. It was shown by using a "spatial index" that the maximum point rainfall in a storm is directly proportional to the surface convergence gradient and size of the convergence area. The size of the convergence area was also found to be one of the most important factors in determining the total rainfall produced by individual storms. Using data from the same Florida experiment, Pielke and Cotton (1977) also related mesoscale kinematic features to rainfall events.

3. Data sources and facilities used

The radar data for this study came from three National Weather Service sites (Pittsburgh, Pennsylvania; Kansas City, Missouri; and Monett, Missouri). These sites are part of the Digitized Radar Experiment (D/RADEX), which was established in late 1971 and early 1972. Basically, each site consists of a WSR-57 (Weather Surveillance Radar-57) interfaced to a NOVA 1200 minicomputer. Additional information concerning D/RADEX can be found in a paper by McGrew (1972). Table 1 summarizes the radar's characteristics. The fundamental resolution is 1 n mi in the radial direction and 2° in the azimuthal direction. The data for a complete radar scope image is archived every 12 min. Each 2° by 1 n mi data bin has a value in the range 0-9 (D/RADEX levels). Table 2 compares the rainfall rates with radar power returned and D/RADEX levels.

The Man-computer Interactive Data Access System (McIDAS), developed by the Space Science and Engineering Center at the University of Wisconsin-Madison, was used for the processing of the radar data. A complete description of the system is given by Smith (1975) and Chatters and Suomi (1975). The system consists of a Datacraft 6024/5 computer, digital disks and I/O devices, interfaced to a color monitor and CRT display by a video display system. An applications program was used to give a frequency distribution of the intensity level of each pixel in an enclosed area. This was used to generate values of area coverage and intensity for each echo.

Hourly airways surface observations were obtained from the archive of the National Severe Storms Forecast Center in Kansas City. The observations used covered the surface grid areas which were slightly larger than the radar coverage areas. Of these observations, there were actually 24 within the Pittsburgh, 14 within the Kansas City and 11 within the Monett radar coverage area.

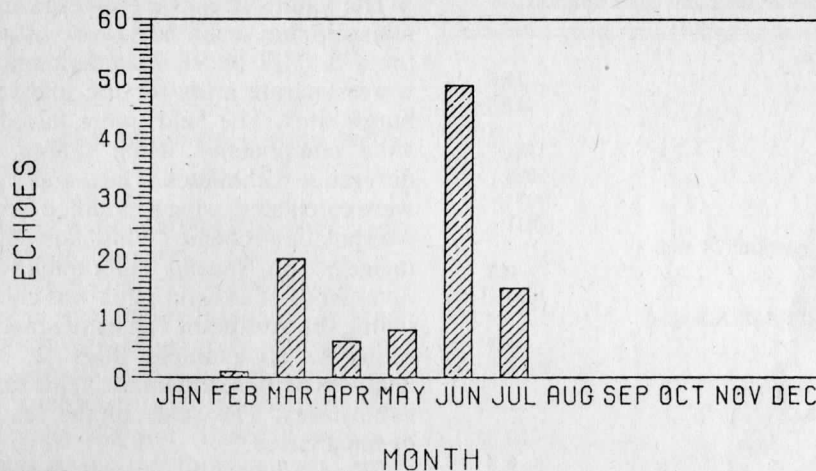


FIG. 1. Number of echoes per month (1976 and 1977 data combined).

4. Methods of analysis of the data

The frontal cases used in this study were generally well defined cold fronts, where the respective radar sites were at least 500 km south of the intersection with the warm front. Quasi-stationary fronts were not used, nor fronts with evidence of a wave near the radar site. Due to logistical and technical difficulties, data were only available for 11 cases of the 30 identified. All cases were between March 1976 and March 1977.

The radar observations used from each of the 11 cases had to meet the criteria that they had at least one (preferably more) distinct echoes which showed somewhat consistent motion and shape. The echoes had to be observed on three consecutive observations, centered on the beginning of an hour. The echoes also had to be completely enclosed by the radar area at all three times. The number of hours of data used from each case varied with the amount of echoes which met the above criteria. Whenever possible, consecutive hours were not used. There was a total of 39 h of observations (three observations used per hour) used from the 11 cases, equally distributed among the three radar sites. From this data set, 99 echoes were studied. Fig. 1 presents a distribution of the number of echoes per month. It is quite clear that the data sampling is strongly biased toward the spring and summer seasons. The average area of the echoes in this study was 1781 km², with half of the echoes having an area <750 km².

The D/RADEX data were converted to a McIDAS compatible format, giving a display of a 1 n mi × 1 n mi Cartesian grid in grey scale form. The grid points were given the value of the D/RADEX data bin in which the points fell. Only D/RADEX levels 2 and above were displayed to give better echo definition.

With each set of radar observations, centered on the hour, a frequency distribution of radar return levels was measured for each echo at the three

times. These three values were averaged to give values of area coverage, maximum intensity and average rainfall rate for the echo. The rainfall rate as given by the relationship in Table 2 was used to estimate average intensity across the echo area. This was done to avoid the logarithmic scaling of radar intensity. For the purposes of this study, the values were not meant to estimate actual rainfall rates. In cases where there was an increase or decrease through the 24 min period, the magnitude of the change was calculated for that period. This was done by subtracting the value 12 min before from that 12 min after the hour. In cases where the trends in the first and second halves of the period were not consistent, the change was ignored. A summary of the means and standard deviations of these parameters is presented as Table 3.

Each of the echoes were classified in five ways: position with respect to the front, relationship with respect to other echoes (in a line, isolated or embedded in a larger area of lighter precipitation), shape (banded or nonbanded), area coverage and geographic location. Table 4 shows the number of echoes in each category.

The classification with respect to frontal position consisted of determining whether the echo was prefrontal, frontal or postfrontal. Frontal echoes in this study are defined as being within 15 n mi of the front.

The second set of classifications was with respect to the type of arrangement the echo was in with other echoes. A line of echoes is defined as several meso-scale areas of precipitation, forming an elongated area of length to width ratio $\geq 5:1$. Any echo which followed the above definition, or was part of such a feature, was classified as line. If the echo was not part of a line, and was not attached to any other echoes, it was classified as isolated. Echoes which were not part of lines, but were embedded in a larger area of lighter precipitation (D/RADEX level

TABLE 3. Summary of the radar echo statistics.

Equivalent radius (km)	
Average	23.8
Median	15.5
Area coverage (km ²)	
Average	1781
Standard deviation	3083
Minimum	54
Maximum	17811
Change of area coverage [km ² (24 min) ⁻¹]	
Average	-0.3
Standard deviation	1033
Maximum intensity (D/RADEX levels)	
Average	4.1
Standard deviation	1.5
Change of maximum intensity [D/RADEX levels(24 min) ⁻¹]	
Average	+0.06
Standard deviation	0.8
Average rainfall rate (mm h ⁻¹)	
Average	2.54
Standard deviation	2.55
Change of rainfall rates [mm h ⁻¹ (24 min) ⁻¹]	
Average	+0.29
Standard deviation	1.4

1) were classified conglomerate. These echoes were sometimes quite close to other mesoscale areas in the same general pattern.

The third classification was simply whether the echo was banded or not. A banded echo is defined here as having a length to width ratio of at least 2:1, as opposed to the greater ratio associated with lines of echoes. Banded echoes may or may not be echoes which are part of lines.

The area coverage classification consisted of separating the larger (>750 km²) and smaller echoes (<750 km²). The breakpoint of 750 km² was chosen because it split the total sample in half.

The geographic classification simply separated the Pittsburgh radar site echoes from the two Midwestern radar site echoes.

TABLE 4. Number of echoes in each classification.

Category	Number of echoes
All	99
Midwest	65
Pittsburgh	34
Prefrontal	62
Frontal	21
Postfrontal	16
Line	43
Isolated	31
Conglomerate	25
Banded	54
Nonbanded	45
Large area	50
Small area	49

The values of surface divergence, divergence of moisture flux and relative vorticity were calculated for a 0.5° 18 by 18 latitude/longitude grid. There were separate grids for the midwestern and Pittsburgh sites. The fields were based on the u and v wind components, using simple, centered finite-difference techniques. The u and v grid-point values were calculated using a modified Cressman weighted interpolation scheme (Whittaker, 1976). This method included no special smoothing techniques. The divergence of moisture flux was calculated by multiplying the grid-point values of u and v by the mixing ratio. As an example, Figs. 2, 3 and 4 present analyses of these kinematic fields for one of the radar echo cases. The scale of the features are typical of most cases.

Using an equally spaced distribution of points throughout the echoes, values of the surface parameters were interpolated from grid-point data using an overlapping polynomial technique (Whittaker and Petersen, 1977). The point values were then averaged to give a value for the echo area. The mean values and standard deviations for the surface parameters in the echo areas are presented in Table 5.

The above procedures were repeated with surface data 1 h before the time of the echo. Thus, the echo parameters were compared to values of surface divergence and vorticity 1 h before the echo moved into that area. Values were also calculated for the surface parameters in the echo relative to the mean for the whole grid. The average grid-point

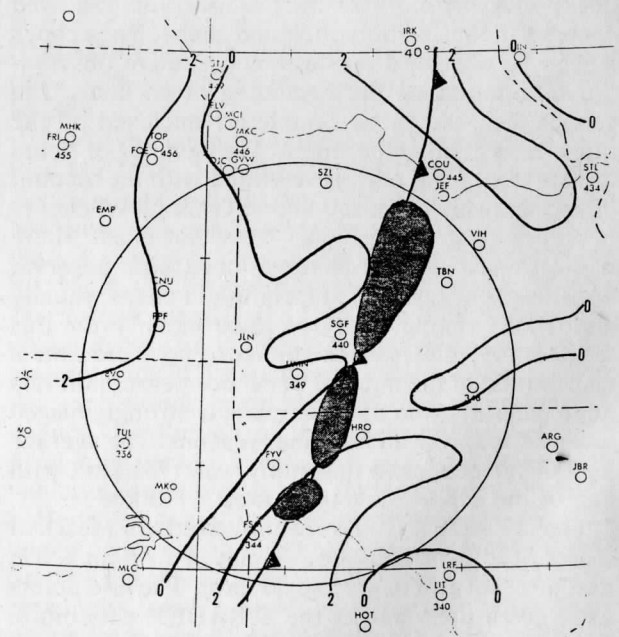


FIG. 2. Surface divergence (10^{-5} s^{-1}) analysis, 1500 GMT 18 April 1976, for the Monett, Missouri radar area. (Shaded areas denote radar echoes.)

value was subtracted from the value of the surface parameter associated with the echo.

5. Relationship of echo parameters with surface kinematic fields

When the various echo parameters were compared with the surface kinematic fields, only a few of the echo parameters gave significant results. The echo parameters of maximum intensity, average rainfall rate and change of average rainfall rate correlated with many of the surface fields used. The area coverage, change of area coverage and change of maximum intensity did not correlate with any surface parameters using the total sample. However, there were a few marginally significant correlations using the echo categories discussed in the previous section. Several categories of echoes did not show any significant correlations at all. These included the Pittsburgh echoes (except for one marginally significant correlation) and the prefrontal, frontal and conglomerate echo categories.

In the following subsections, correlation statistics involving each of the three echo parameters which showed significant results will be discussed. The statistics applying to the total sample will be presented in detail. Only the more important points with the individual categories of echoes will be discussed.

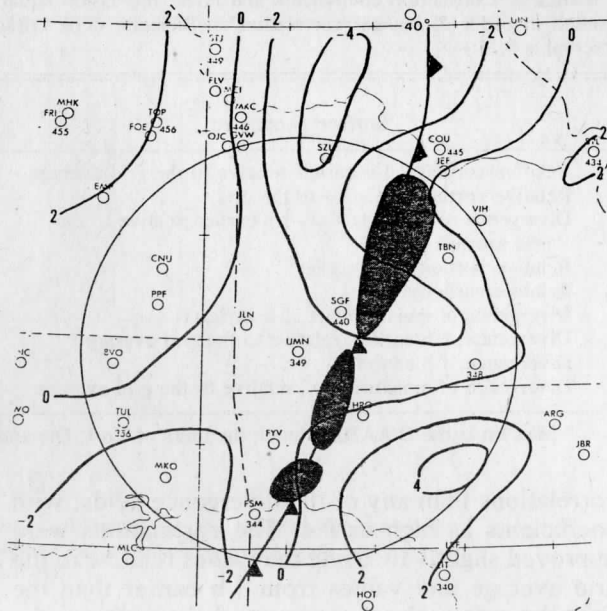


FIG. 4. Surface relative vorticity (10^{-5} s^{-1}) analysis, 1500 GMT 18 April 1976, for the Monett, Missouri radar area. (Shaded areas denote radar echoes.)

a. Maximum intensity

Table 6 shows the correlation coefficients and regression equations for the relationships involving maximum intensity. Relative vorticity gave better

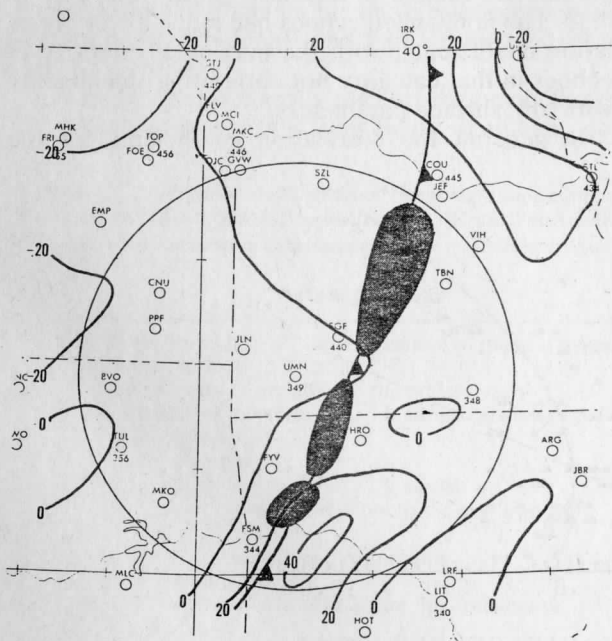


FIG. 3. Surface divergence of moisture flux (10^{-5} s^{-1}) analysis, 1500 GMT 18 April 1976, for the Monett, Missouri radar area. (Shaded areas denote radar echoes.)

TABLE 5. Summary of surface parameters.

Surface parameter	Mean (10^{-5} s^{-1})	Standard deviation (10^{-5} s^{-1})
Divergence	-0.47	2.40
One hour earlier	-0.66	2.73
Change in 1 h	0.19	2.03
Relative to the grid average	-0.29	2.29
One hour earlier, relative to the grid average	-0.49	2.68
Change in 1 h relative to the grid average	0.20	2.00
Divergence of moisture flux	-7.13	28.80
One hour earlier	-8.95	33.52
Change in 1 h	1.82	24.71
Relative to the grid average	-5.46	27.56
One hour earlier, relative to the grid average	-7.52	33.08
Change in 1 h, relative to the grid average	2.05	24.28
Relative vorticity	0.87	2.36
One hour earlier	0.70	2.59
Change in 1 h	0.17	1.76
Relative to the grid average	0.72	2.24
One hour earlier, relative to the grid average	0.56	2.50
Change in 1 h, relative to the grid average	0.16	1.76

TABLE 6. Correlation coefficients and linear regression equations for the maximum intensity and various surface parameters, ranked in order of highest correlation coefficients. (The critical coefficient magnitude for significance at the 95% confidence interval is 0.23.)

Surface parameter	Linear regression equation*	Correlation coefficient
Relative vorticity, 1 h earlier relative to the grid average	Max Int = 4.04 + 0.24 (Vort)	0.40
Relative vorticity, relative to the grid	Max Int = 3.90 + 0.27 (Vort)	0.40
Divergence of moisture flux, 1 h earlier relative to the grid average	Max Int = 4.05 - 0.02 (DivMF)	-0.38
Relative vorticity, 1 h earlier	Max Int = 4.04 + 0.2 (Vort)	0.35
Relative vorticity	Max Int = 3.89 + 0.22 (Vort)	0.34
Divergence of moisture flux, 1 h earlier	Max Int = 4.04 - 0.015 (DivMF)	-0.34
Divergence, 1 h earlier, relative to the grid average	Max Int = 4.09 - 0.18 (Div)	-0.33
Divergence, 1 h earlier	Max Int = 4.08 - 0.15 (Div)	-0.27
Divergence of moisture flux, relative to the grid average	Max Int = 4.04 - 0.16 (DivMF)	-0.24

* Max Int is the D/RADEX level; the units of Vort, Div and DivMF are 10^{-5} s^{-1} .

correlations than any of the divergence fields, with coefficients as high as 0.4. The correlations were improved slightly by using the values relative to the grid average and values from 1 h earlier than the time the radar echo was observed. In addition, the divergence of moisture flux correlated better than the divergence of the wind field alone.

The relative vorticity gave positive correlations with the maximum intensity, while the divergence parameters correlated negatively. This means that the stronger the relative vorticity is in the area to which an echo is moving, or is already located, the higher the maximum intensity associated with the echo. The negative correlation with the divergence is similar in that the more intense echoes will have had stronger convergence in the same area an hour earlier.

A scatter diagram is presented as Fig. 5, showing the relationship of the relative vorticity 1 h earlier than the echo time, relative to the grid average, to the maximum intensity. The distribution of points

seems to be better described by a nonlinear relationship than the least-squares regression line. Fig. 6 shows the distribution of correlation coefficients for the same relationship of Fig. 5, for each of the categories showing significant correlations. The most statistically significant categories to be noted are the banded and larger area categories. Both of these categories had much higher correlations than their counterparts, namely, the nonbanded category, which showed no significant correlations, and the smaller area category.

The banded echoes gave the highest correlation coefficients of any of the echo categories except for the very limited sample of postfrontal echoes. The coefficients which were significant with the surface parameters ranged in absolute value from 0.34 to 0.58. The nonbanded echoes had much lower correlation coefficients, with the maximum intensity of echoes in that category not correlating significantly with any surface parameters.

In general, the correlation coefficients for the

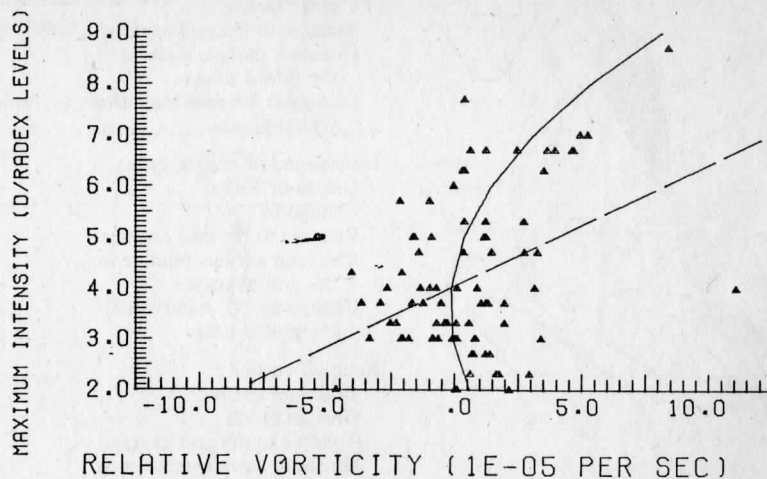


FIG. 5. Scatter diagram of maximum intensity versus the relative vorticity 1 h earlier than the echo, relative to the average grid value of vorticity.

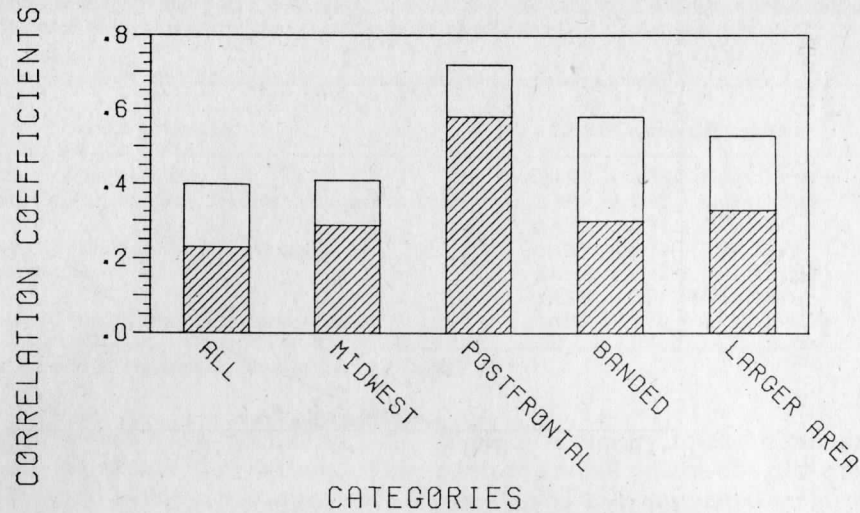


FIG. 6. Distribution of the correlation coefficients for the relationship shown in Fig. 5 by echo category. (Shaded areas denote values which the correlation coefficients must exceed to be significant at the 95% level.)

larger (>750 km²) echoes were more than twice those of the small echoes, each having the same sample size. The coefficients which were significant with the surface parameters ranged in absolute value from 0.33 to 0.56. Interestingly, the few cases in which the maximum intensity did correlate significantly to a surface parameter for the smaller echoes were cases in which the larger echoes correlated exceptionally poorly. These were the change of divergence of moisture flux during the past hour, and that change relative to the average grid value. The correlation coefficients for these relationships were marginally significant, and had values of 0.39 and 0.38, respectively.

The reason for many of the correlation coefficients with the midwestern echoes being significant, com-

pared with none for the Pittsburgh echoes, is not understood. This may be due solely to the small sample size there, or to some orographic effects. Similar questions arise when trying to explain why the postfrontal echoes correlated significantly, but not the frontal or prefrontal. All of the postfrontal echoes were observed in the midwest sites. These same problems also arise with the other echo parameters to be discussed.

b. Average rainfall rate (radar estimated)

The average rainfall rates of the echoes showed the best correlation to surface parameters of any of the echo parameters tested. The correlations, as shown in Table 7, are similar to those of the maxi-

TABLE 7. Correlation coefficients and linear regression equations for the average rainfall rate and various surface parameters, ranked in order of highest correlation coefficients. (Critical correlation magnitude for significance at the 95% confidence interval is 0.23.)

Surface parameter	Linear regression equation*	Correlation coefficient
Relative vorticity, 1 h earlier, relative to the grid average	ARR = 2.38 + 0.58 (Vort)	0.53
Relative vorticity, 1 h earlier	ARR = 2.34 + 0.52 (Vort)	0.50
Relative vorticity, relative to the grid average	ARR = 2.23 + 0.56 (Vort)	0.47
Divergence of moisture flux, 1 h earlier relative to the grid average	ARR = 2.44 - 0.035 (DivMF)	-0.43
Relative vorticity	ARR = 2.19 + 0.48 (Vort)	0.42
Divergence of moisture flux, 1 h earlier	ARR = 2.41 - 0.03 (DivMF)	-0.40
Divergence, 1 h earlier, relative to the grid average	ARR = 2.5 - 0.39 (Div)	-0.39
Divergence, 1 h earlier	ARR = 2.47 - 0.35 (Div)	-0.35
Change of divergence of moisture flux	ARR = 2.64 + 0.04 (DivMF)	0.34
Change of divergence	ARR = 2.62 + 0.45 (Div)	0.33
Change of divergence of moisture flux, relative to the grid average	ARR = 2.63 + 0.04 (DivMF)	0.33
Change of divergence, relative to the grid average	ARR = 2.62 + 0.43 (Div)	0.32
Divergence of moisture flux, relative to the grid average	ARR = 2.47 - 0.02 (DivMF)	-0.25

Units of average rainfall rate (ARR) are mm h⁻¹, those of Vort, Div and DivMF 10⁻⁵ s⁻¹.

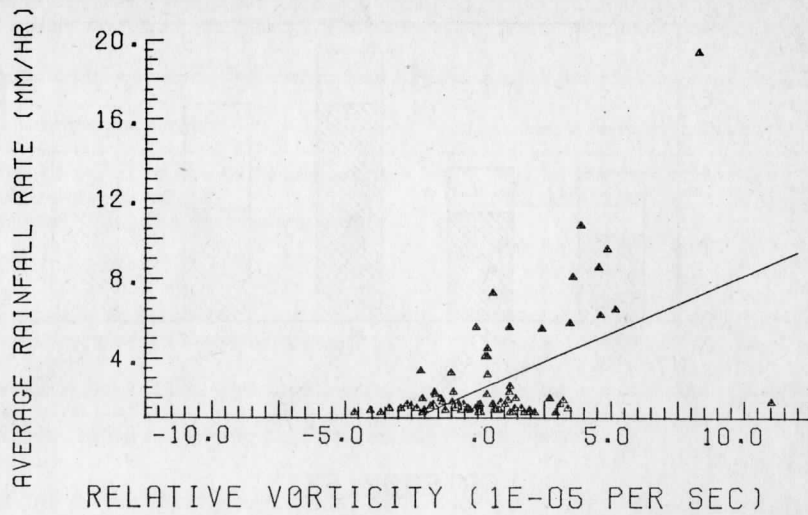


FIG. 7. Scatter diagram of average rainfall rate versus the relative vorticity 1 h earlier than the echo, relative to the average grid value of vorticity.

mum intensity in that the relative vorticity showed the best relationship among all of the surface parameters. Stronger positive vorticity is associated with higher average rainfall rates. The divergence parameters correlated negatively except for the change of divergence which had a positive correlation. These relationships are all consistent with the idea that higher average rainfall rates are associated with stronger convergence in the area to which the echo is moving. As the echo moves into the area, the wind field becomes more divergent at the surface, accounting for the positive change of divergence over the hour. It is interesting to note, though, that the divergence of the wind field alone did not show significant correlation with either the maximum intensity or the average rainfall rate.

A scatter diagram for relative vorticity, 1 h earlier than the echo time and relative to the grid average, versus the average rainfall rate is given in Fig. 7. The plot shows that a wide range of surface vorticities are associated with echoes which have low average rainfall rates. The relationship becomes more organized as the average rainfall rate increases. Fig. 8 shows much the same type of distribution of correlation coefficients among the echo categories as did Fig. 6 with maximum intensity.

As before, the banded and larger echoes showed much better correlation with surface parameters than the nonbanded and smaller echoes. The nonbanded echoes did show marginally significant correlation with the relative vorticity at the same time as the echo, and the same relative to the grid aver-

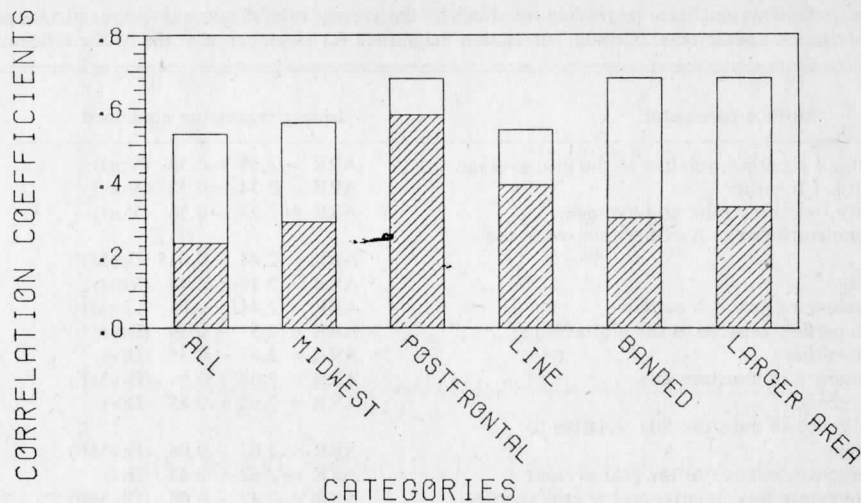


FIG. 8. Distribution of correlation coefficients for the relationship shown in Fig. 7, by echo category. See Fig. 6.

TABLE 8. Correlation coefficients and linear regression equations for the change of average rainfall rate and various surface parameters, ranked in order of highest correlation coefficients. (Critical correlation value for significance at the 95% confidence interval is 0.24.)

Surface parameter	Linear regression equation*	Correlation coefficient
Change of divergence of moisture flux	$\Delta ARR = 0.33 + 0.03 (\text{DivMF})$	0.42
Change of divergence of moisture flux, relative to the grid average	$\Delta ARR = 0.32 + 0.03 (\text{DivMF})$	0.41
Change of divergence	$\Delta ARR = 0.31 + 0.29 (\text{Div})$	0.38
Change of divergence, relative to the grid average	$\Delta ARR = 0.31 + 0.29 (\text{Div})$	0.37
Divergence of moisture flux	$\Delta ARR = 0.32 + 0.02 (\text{DivMF})$	0.29
Divergence	$\Delta ARR = 0.31 + 0.16 (\text{Div})$	0.26
Divergence of moisture flux, relative to the grid average	$\Delta ARR = 0.30 + 0.01 (\text{DivMF})$	0.26

* Units of ΔARR are $\text{mm h}^{-1}(24 \text{ min})^{-1}$, those of Div and DivMF 10^{-5} s^{-1} .

age. But, the banded echoes had a much more substantial number of significant correlations. The larger echoes, as they did with the maximum intensity, generally correlated more than twice as well as the smaller ones. Again, smaller echoes did have a few significant correlations, all of which were with surface parameters which correlated poorly with the larger echoes. Those categories were the changes of divergence and divergence of moisture flux, and those parameters relative to the grid averages. The correlation coefficients ranged from 0.40 to 0.48, where the critical correlation coefficient for significance was 0.33.

c. Change of average rainfall rate

The relationship of the change of average rainfall rate to the surface parameters is not nearly as consistent as the two preceding relationships, but it is considered worth mentioning. The correlation coefficients and regression equations are listed in

Table 8. Contrary to the maximum intensity and average rainfall rate results, the change of the average rainfall rate correlated quite poorly to any of the relative vorticity parameters. Apparently, the relative vorticity best relates to the actual values of these echo parameters at specific times, while fields such as the change of the divergence of moisture flux better relate to the changes of echo parameters in time. The change of the divergence fields did give better relationships with the average rainfall rate than the divergence fields at either the time of the echo or the previous hour. This shows that as an echo moves into an area, the more that echo is increasing its average rainfall rate, the more divergent the wind field becomes. This seems consistent considering the stronger downdrafts which would be associated with the more intense rainfall.

A scatter diagram of the change of divergence of moisture flux over the 1 h period preceding the time of the echo versus the change of the average

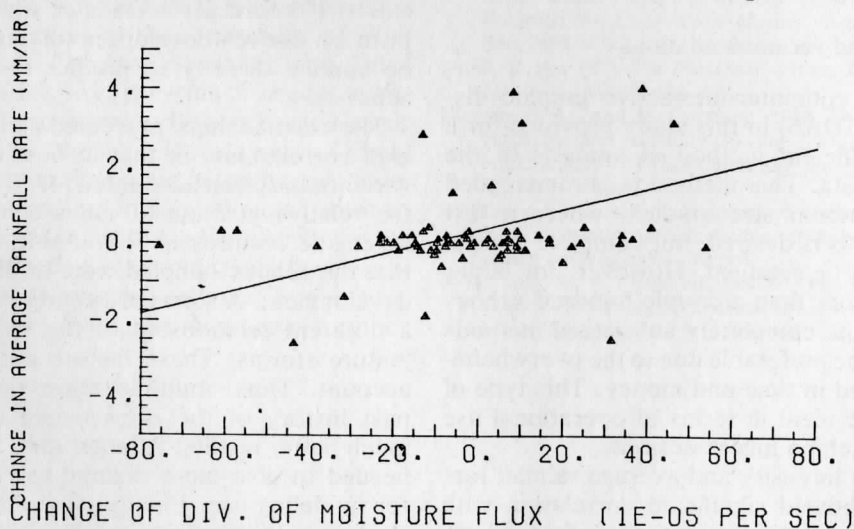


FIG. 9. Scatter diagram of the 24 min change of average rainfall rate versus the 1 h change of divergence of moisture flux.

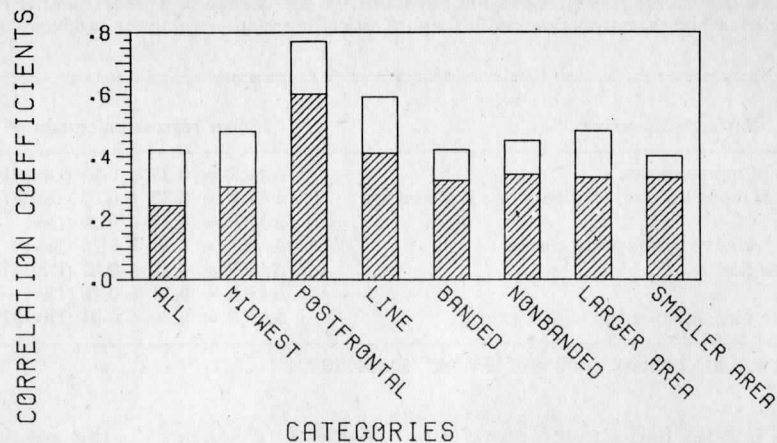


FIG. 10. Distribution of correlation coefficients for the relationship shown in Fig. 9, by echo category. See Fig. 6.

rainfall rate during the 24 min period the echo was observed is presented as Fig. 9. As can be seen, this relationship is not described very well by the linear regression equation. The change of rainfall rate values tend to be concentrated around zero, while the divergence values show much better distribution.

The distribution of significant correlation coefficients by each category is shown in Fig. 10. The reason for the significant correlations in the midwestern and postfrontal echo categories as opposed to none in their corresponding categories remains a mystery. The echoes which are part of lines continue to show up occasionally with significant correlations. In contrast to the previous echo parameters, there were no substantial differences between the banded and nonbanded categories and the larger and smaller echo categories for the change of the average rainfall rate.

6. Conclusions and recommendations

The use of a computer-interactive graphic display system (McIDAS) in this study provided for a very fast and efficient method of analysis of the digitized radar data. This method is recommended for small to medium size studies, where a fast method of analysis is desired, but complete control of the data is to be retained. However, for larger studies where more than a couple hundred echoes are to be used, the completely automated methods would probably be preferable due to the overwhelming costs involved in time and money. This type of system would be ideal in terms of operational use where a man-machine mix is desired.

The maximum intensity and average rainfall rate of the echoes showed significant correlation with many of the surface parameters tested, particularly the relative vorticity. These correlations were im-

proved by using values of the surface fields for the area covered by the echo, 1 h before it arrived there; and also by finding the value relative to the grid average. Banded echoes had much better correlations than nonbanded ones, with the same true for large echoes compared with small echoes ($<750 \text{ km}^2$). The divergence of moisture flux correlated better than the divergence of the wind alone. While the change of average rainfall rate for the echoes did not give as good relationships as the other two radar parameters, some significant correlations were found, particularly with the change of divergence of moisture flux.

When applying the relationships discussed in this study to operational forecasting, caution must be exercised. Since there were no dry cases (no radar echoes) used in the analysis, the relationships presented apply only in cases where an echo already exists. If a forecast is made of where the echo will be in 1 h, the relationships involving the time lag can be applied directly to predict the intensity characteristics.

The relationships presented here did not show high correlations, in that at best only 25% of the variance has been accounted for. One of the reasons the relative position of radar echoes and surface kinematic features is so variable may be the fact that the echoes sampled were at different stages of development. A storm in its early stages would have a different relationship to the surface fields than mature storms. These factors must be taken into account. Thus, multiple regression involving the past history of the echo would most likely give much better results. A larger data sample would be needed to give more definite regression equations for modeling use. Finally, since the results of this study point strongly to the idea that there is a time lag between occurrences on the surface and what

happens in the clouds, studies should be made to examine this in more detail.

There are many effects which disturb the surface wind field, making it very difficult to generate accurate divergence or vorticity fields. One solution which would give better results would be to use the wind field at or slightly below cloud level. The present radiosonde network is not of sufficient density to provide such data, and probably never will be. One possible source of such data is from satellites. Currently, winds are being generated from satellite picture loops. If enough clouds could be tracked in the area of the precipitation, detailed wind fields at the cloud level could be used for generating divergence and vorticity fields. There are undoubtedly many problems involved, but it seems to be worth pursuing. Another source would be by a dense network of remote sounding devices such as lidar.

In any case, it appears possible to make reasonable forecasts of the movement of radar echoes and forecast their intensity based on synoptic-scale parameters and the echoes' past histories. In future years, when fine-resolution digitized radar is installed nationwide, endless amounts of data should be available for massive statistical analyses.

Acknowledgments. The first author is deeply indebted to the National Weather Service for providing one year of graduate study at the University of Wisconsin, as well as to the many people who assisted in completing the research. We are grateful to Professors Eberhard W. Wahl and Gerald F. Herman for their constructive criticism. Paul Wofsy and Nancy Nagle of the Office of Technical Services, National Weather Service, and Horace Hudson of the National Severe Storms Forecast Center helped by furnishing data. Donald Wylie, John Stout and Gary Chatters of the Space Science and Engineering Center at the University of Wisconsin, as well as Thomas Whittaker and Peter Guetter of the University, gave much needed computer programming assistance. Robert Elvander and Robert Saffle of the Systems Development Office, National Weather Service, were helpful consultants in the use of digitized radar data. We also want to thank Thomas Koehler for his assistance in the research. The constructive comments from the anonymous reviewers were most appreciated. Funding for this research came from the National Weather

Service and National Science Foundation Grant ATM77-20231.

REFERENCES

- Austin, J. M., and R. H. Blackmer, Jr., 1956: The variability of cold front precipitation. *Bull. Amer. Meteor. Soc.*, **37**, 447-453.
- Boucher, R. J., and R. Wexler, 1961: The motion and predictability of precipitation lines. *J. Meteor.*, **18**, 160-171.
- Byers, H. R., and L. J. Braham, 1949: *The Thunderstorm*. U.S. Govt. Printing Office, Washington, DC, 287 pp.
- Chatters, G. C., and V. E. Suomi, 1975: The applications of McIDAS. *IEEE Trans. Geosci. Electron.*, **GE-13**, 137-146.
- Cox, M. K., 1959: The distribution and variability of cold-front precipitation. *Bull. Amer. Meteor. Soc.*, **40**, 477-480.
- Cruz, L. A., 1973: Venezuelan rainstorms as seen by radar. *J. Appl. Meteor.*, **12**, 119-126.
- Elvander, R. C., 1976: An evaluation of the relative performance of three weather radar echo forecasting techniques. *Preprints 17th Conf. Radar Meteor.*, Seattle, Amer. Meteor. Soc., 526-532.
- Harper, W. G., and J. G. D. Beimers, 1958: The movement of precipitation belts as observed by radar. *Quart. J. Roy. Meteor. Soc.*, **84**, 242-249.
- McGrew, R. G., 1972: Project D/RADEX (Digitized Radar Experiments). *Preprints 15th Radar Meteor. Conf.*, Urbana, Amer. Meteor. Soc., 101-106.
- Mielke, K. B., and D. D. Houghton, 1977: An analysis of radar echo systems for the upper midwestern United States. *J. Appl. Meteor.*, **16**, 833-843.
- Myers, J. N., 1964: Preliminary radar climatology of central Pennsylvania. *J. Appl. Meteor.*, **3**, 421-429.
- Newton, C. W., and J. C. Fankhauser, 1964: On the movements of convective storms, with emphasis on size discrimination in relation to water-budget requirements. *J. Appl. Meteor.*, **3**, 651-668.
- Pielke, R. A., and W. R. Cotton, 1977: A mesoscale analysis over south Florida for a high rainfall event. *Mon. Wea. Rev.*, **105**, 342-362.
- Saffle, R. E., 1976: D/RADEX products and field operation. *Preprints 17th Conf. Radar Meteor.*, Seattle, Amer. Meteor. Soc., 555-559.
- , and D. R. Greene, 1978: The role of radar in the flash flood watch warning system: Johnstown reexamined. *Preprints 18th Conf. Radar Meteor.*, Atlanta, Amer. Meteor. Soc., 468-473.
- Smith, E. A., 1975: The McIDAS system. *IEEE Trans. Geosci. Electron.*, **GE-13**, 123-136.
- Ulanski, S. L., and M. Garstang, 1978: The role of surface divergence and vorticity in the life cycle of convective rainfall. Part I: Observation and analysis. *J. Atmos. Sci.*, **35**, 1047-1062.
- Whittaker, T. M., 1976: A simplified grid interpolation scheme for use in atmospheric budget studies. M.S. thesis, University of Wisconsin, 42 pp.
- , and R. A. Petersen, 1977: Objective cross-sectional analyses incorporating thermal enhancement of the observed winds. *Mon. Wea. Rev.*, **105**, 147-153.

Mesoscale Wind Fields for a Severe Storm Situation Determined from SMS Cloud Observations

THOMAS A. WILSON¹ AND DAVID D. HOUGHTON

Department of Meteorology, University of Wisconsin, Madison 53706

(Manuscript received 26 February 1979, in final form 24 May 1979)

ABSTRACT

An attempt is made to obtain fully three-dimensional mesoscale wind fields from satellite cloud displacement data for an area over the continental United States. A method to derive such fields and their likely accuracy is discussed prior to the presentation of a test case for 30 October 1974. The computed divergence and vertical motion fields are consistent with features of the observed mesoscale weather systems, particularly the locations of subsequent severe convective storms.

1. Introduction

Since the advent of satellite imagery in the 1960's, numerous attempts have been made to extract useful quantitative data from the images. This activity has been extended to the measurement of cloud time-displacement vectors using sequences from geostationary satellites. At the University of Wisconsin, the development of a highly automated data handling facility, McIDAS (Suomi, 1975), has made it possible to obtain large numbers of displacement vectors rapidly in a precise manner.

The relationship between these vectors and the atmospheric velocity vectors has been a matter of great interest and discussion. Establishment of the correspondence between the two would allow for tremendous enhancement of the description of the large-scale wind fields over much of the earth, particularly ocean areas and, for the first time, determination of the mesoscale wind fields above the earth's surface.

Numerous studies have been made relating cloud motion vectors to large-scale wind fields. Hubert and Whitney (1971) summarized the overall correspondence of the two forms of data for tropical regions. At synoptic scales, cloud (motion) vectors have gained the acceptance of being incorporated with the daily National Weather Service (NWS) tropical analyses. On the other hand, mesoscale velocity fields obtained from the cloud-displacement technique have had far less examination.

At the mesoscale the accuracy of cloud displacement vectors is more difficult to assess than at synoptic scales. Absolute errors imply larger errors

in differentiated quantities such as vorticity, divergence, and vertical motion because of the shorter length scales involved. However, these quantities tend to have larger magnitudes so that the signal-to-noise ratio is not necessarily made larger. Diagnostic consistency checks between the velocity field and other variables are not available as for the large-scale situation. Finally, there is little scale-compatible velocity data from other sources such as rawinsondes with which to "directly" calibrate the satellite image results. Even if individual vectors turn out to have relatively large errors there is hope that, with sufficient density of data points, ensemble averages would provide useful information.

This study summarizes one of the first attempts to obtain three-dimensional mesoscale wind fields from satellite cloud data for a midlatitude situation. Analysis was focused on the satellite imagery of a severe storm event in northern Texas. Horizontal cloud displacement vectors were derived with the intent to cover the region in three dimensions throughout the troposphere. Objective analysis and diagnostic methods were used to deduce horizontal fields of divergence and vertical motion from the basic wind data. In recognition of the basic questions of the validity of the cloud displacement vectors, a short discussion of the accuracy and correspondence of cloud motions to air motions is presented in the following section as general background material.

2. The accuracy and correspondence of cloud motions to air motions

Cloud displacement vectors and air motions of the same time scale differ due to errors in any given

¹ Current affiliation: Environmental Data Service, NOAA, Washington, DC 20235.

TABLE 1. Summary of error estimates for satellite cloud wind and rawinsonde wind data appropriate for the case study presented here.

Error type	Vector error magnitude		Reference
	rms (m s^{-1})	Variance ($\text{m}^2 \text{s}^{-2}$)	
Satellite cloud motion vectors			
Navigation	0.4	0.2	Wilson (1976)*
Single pixel tracking	1.1	1.2	Wilson (1976)
Image resolution	0.6	0.4	Wilson (1976)
Height assessment	2.5	6.3	Wilson (1976)
Overall tracking random error (cumulative effect of all above except navigation)	2.8	7.9	
Rawinsonde wind data			
Rawinsonde	1.75	3.1	Representative value from Bengtsson (1975) and U.S. Air Force (1963)
Temporal variability over 90 minutes	2.2	4.6	Reiter (1961)
Spacial variability over 180 km	3.8	14.5	Reiter (1961)
Overall random error (cumulative effect of the above three)	4.7	22.2	

* Wilson (1976) presented these error estimates as range values. These were converted to the variance form shown here by using normal distribution relationships for a sample of five.

cloud tracking method and non-representative cloud motions. Measurements of these two factors are reviewed below. Their combined effect, the total error of the cloud displacement vectors, is estimated for the vectors of this study.

a. Accuracy of tracking via satellite

The precision with which a target can be located and tracked in the troposphere via satellite is limited by error due to four sources: image navigation, image resolution (temporal and spatial), the tracking method used, and the accuracy of the target height determination. Suchman and Martin (1976) have stated that the overall accuracy obtained with the McIDAS system, using equatorial data, is "within the accuracy of currently available ground truth." Using the same system, Wilson (1976) discussed the four sources of error separately and estimated their magnitude. Table 1 summarizes the magnitudes for the test case of this paper. It should be noted that of the four errors, all but the first should have a major random component and will often be partially offsetting.

For this north Texas case, the sum of the variances of the three random errors is estimated to be $7.9 \text{ m}^2 \text{ s}^{-2}$, giving a random error standard deviation of 2.8 m s^{-1} . The navigational error adds an additional increment of error to this figure, an amount nearly identical for all wind vectors. In this paper we are interested in divergence calculations. In such calculations any bias which is uniform throughout the entire wind field will be eliminated. Consequently, for the purposes of this paper the navigational error is not included in the system error figure, although

the use of objective analysis will distort slightly the originally uniform navigational bias.

In view of the importance of target height determination, a brief discussion of the McIDAS method used for the North Texas case is perhaps in order before proceeding. The method used incorporates the visible and infrared satellite images and the relative angles of the satellite and sun to the target cloud. The brightness of a target cloud in the visible image is correlated with an appropriate cloud thickness via a lookup table. Knowing the cloud thickness, its infrared emissivity is then calculated. In this last step, adjacent areas are compared to account for the influence of partial cloudiness on a sub-pixel scale. In actuality the tracers chosen for the North Texas case were distinct in the visible image and consequently quite thick with emissivities near unity. The height program searches for the brightest (coldest) infrared pixel of the cloud and calculates temperature from that. For such calculations, the program accuracy is estimated at $3\text{--}5^\circ\text{C}$ where the sensor picks up radiation from only one cloud level. For the North Texas case, five sequential height determinations made in the construction of each cloud vector were screened to determine that the sensor was indeed picking up radiation from but one level.

b. Non-representative cloud motions

The correspondence of cloud motions to air motions is crucial to the work of this paper. Although the expectable error cannot be proven, a reliable estimate must nonetheless be found. In addition, since the cloud motion vectors in this study are

derived from satellite imagery and assigned to the cloud-top height, the non-representativeness of the cloud motions at the cloud-top height with respect to ambient flow at *the same height* must be estimated for the vectors measured in this study. The authors formulate an estimate as follows.

Non-representative cloud motion has been investigated using a variety of cloud viewing platforms, two of which are airplanes and satellites. In the former case, measurements of the ambient air motion have been taken in and about the cloud with instrumented aircraft while various aspects of the cloud motion were simultaneously observed. In the latter case, cloud motion vectors have been derived from satellite imagery and the accuracy assessed by comparison with nearby radiosonde reports.

Applying the former model, Hasler *et al.* (1977) tracked the geometric centers as viewed from aircraft flying within and above isolated tradewind cumulus with bases at 960 mb, diameters of 3 to 15 km, thicknesses of 360 to 760 mb, and lifetimes generally near 1 h. They found that in 67% of the cases the center of tradewind cumulus clouds moves with a vector difference magnitude of 1.5 m s^{-1} from the wind 150 m above the sea surface, 1.3 m s^{-1} from the wind at the cloud base, 3.6 m s^{-1} from the mid-cloud wind, and 7.0 m s^{-1} from the wind at the cloud top. Using the same aircraft, the authors found that "isolated cirrus clouds moved with a vector difference magnitude of 1.6 m s^{-1} from the mean wind in the cloud layer."

The cloud tracers used in this study are not the geometric centers of large trade wind cumulus lasting 1 h, but rather the leading edge—if possible, and otherwise the geometric center—of a mix of midlatitude cloud types as shown later, generally with lifetimes of 18–25 min and diameters of 3 to 4.5 km. These tracers were selected subjectively from the satellite image loop as being most representative of ambient mesoscale flow at the cloud-top layer, as opposed to lower levels or microscales. Consequently, it is not certain what the work of Hasler *et al.* might imply of the non-representative motion inherent in assigning these tracers to the cloud top height. For this reason, a further consideration using the results of satellite investigations is developed here.

A number of studies have been made comparing satellite-derived vectors with nearby radiosonde reports. Studies by Wiegman *et al.* (1971), Mosher and Sawyer (1976), and Bauer (1976) have found upper bounds of the rms (mean) vector difference magnitude between radiosonde and satellite derived cloud vectors to range from 5.5 to 6.0 m s^{-1} ; or, put another way, the variance between the measurements has been shown to be as large as $36 \text{ m}^2 \text{ s}^{-2}$. A large part of this variance is due to the random combination of satellite tracking error, radiosonde error,

atmospheric variability over the time and over the space of comparison, and nonrepresentative cloud motion. Variance values for the first three of those four, based on range values, are listed in Table 1 for the data of this test case. The three variances sum to $\sim 22 \text{ m}^2 \text{ s}^{-2}$. By deduction, the contribution of nonrepresentative cloud motion to the total variance may be estimated by the difference $36 - 22 \text{ m}^2 \text{ s}^{-2}$, or $14 \text{ m}^2 \text{ s}^{-2}$. The standard deviation of nonrepresentative cloud motion is then approximately 3.7 m s^{-1} . It must be noted that the height error listed in Table 1 is a subjective estimate for this data set only, based upon objective data for 258 wind vectors derived in three Data Systems Tests with McIDAS (Wilson, 1976). With this qualification, it is noted that the 3.7 m s^{-1} figure estimated for non-representative cloud-top motion using the figures of Table 1 is close to the 3.6 m s^{-1} value noted by Hasler *et al.* (1977) as the difference between ambient mid-cloud air flow and motion of the geometric centers of the clouds. It is proposed that, as an estimate, the error due to nonrepresentative motion of the cloud tracers used in this study has an rms value of $\sim 3.7 \text{ m s}^{-1}$.

The thrust of this section has been to assess the accuracy of cloud motion vectors. Standard deviations of error in the horizontal wind fields for the North Texas case have been estimated as 2.8 m s^{-1} due to the mechanical tracking technique and 3.7 m s^{-1} due to the nonrepresentative nature of cloud motions, giving variances of ~ 8 and $14 \text{ m}^2 \text{ s}^{-2}$, respectively. The total variance of the random error is then $22 \text{ m}^2 \text{ s}^{-2}$, from which we derive the standard deviation of the error in our satellite-derived cloud motion vectors to be $\sim 4.7 \text{ m s}^{-1}$.

3. A method to derive three-dimensional wind fields

Using the technological base of McIDAS, the following five-step method was developed to derive three-dimensional wind fields from satellite imagery.

Step 1. From a sequence of images with a good three-dimensional selection of cloud targets, as many horizontal cloud-displacement vectors are measured as possible.

Step 2. The vector sequences are objectively edited and time-averaged into single vectors.

Step 3. These vectors are then grouped into layers according to pressure height. Assigning a vector to an altitude or pressure level (pressure height) is possible as the satellite-derived vectors are determined at the level of cloud-top temperature and a ground-based sounding will relate that temperature to altitude and pressure.

Step 4. An objective analysis scheme is used to extrapolate vectors to the mid-level of the respective layers and to a regular array of grid positions.

Step 5. Vertical motion is calculated by using the

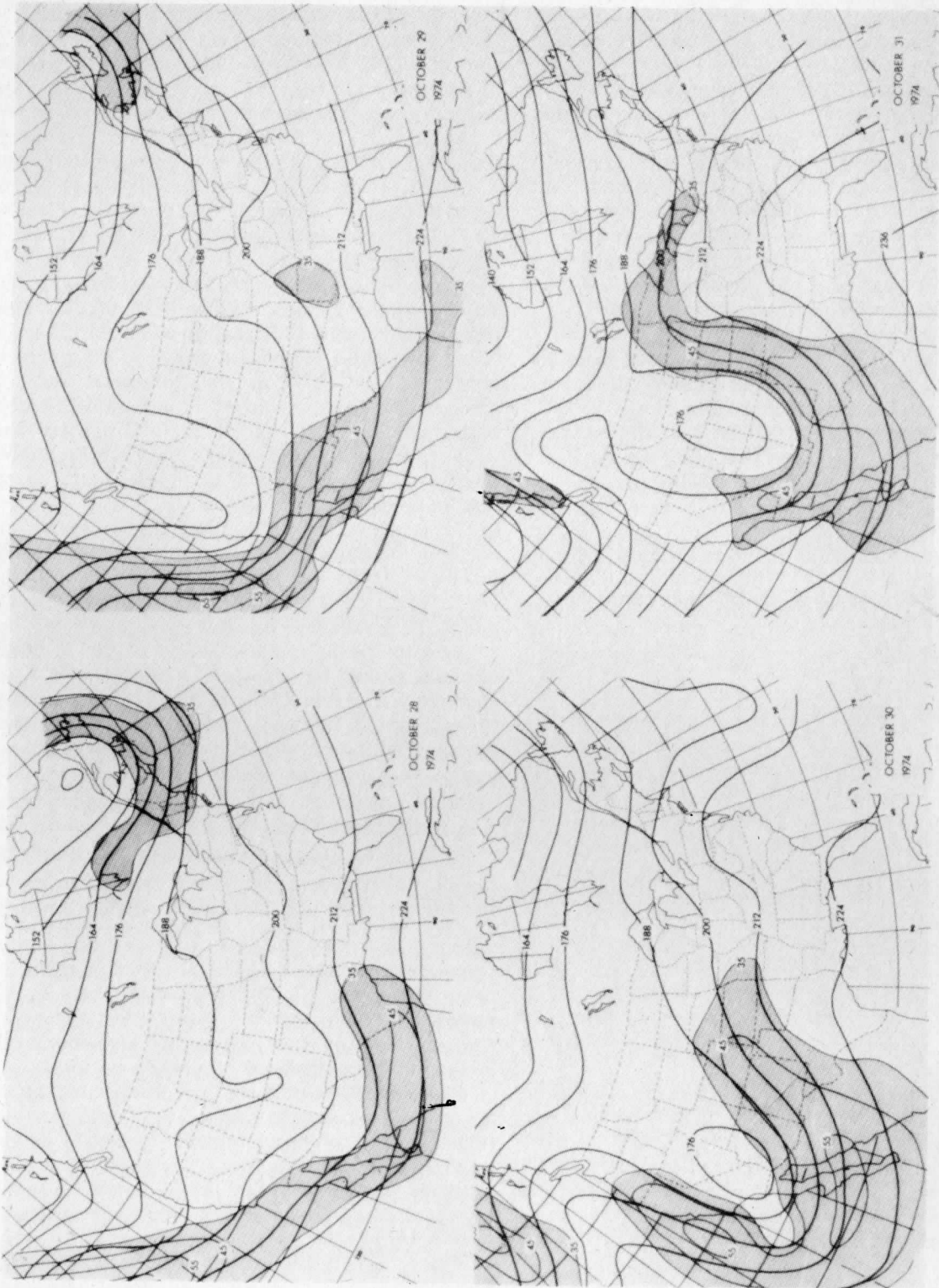


FIG. 1. The 0000 GMT NWS height analyses at 200 mb (dam) for the case study. Isotachs ($m s^{-1}$) are shown by the thinner lines with shading for values $\geq 35 m s^{-1}$.

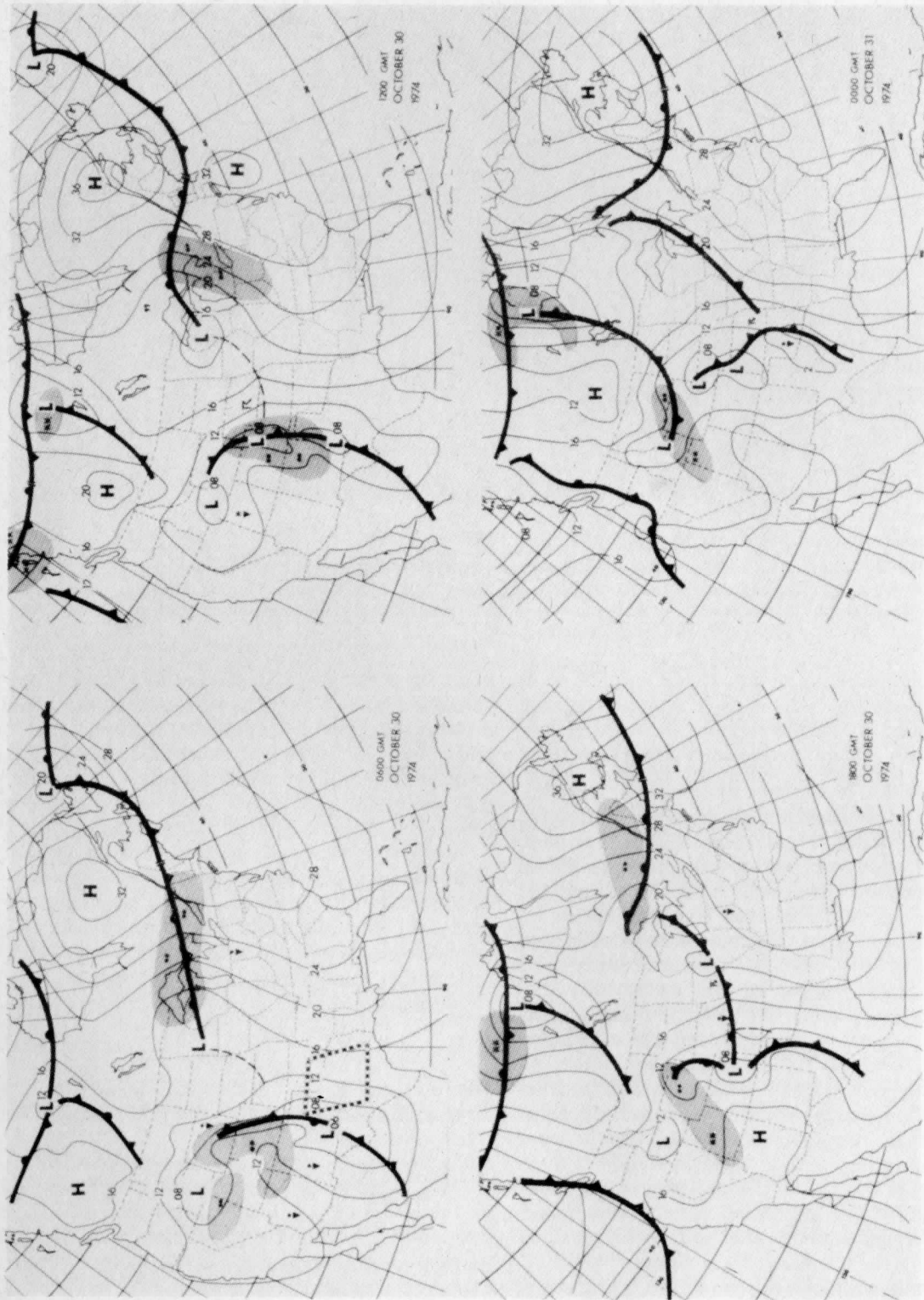


FIG. 2. NWS surface analyses for the time period of the case study. Contours are for sea level pressure with an interval of 4 mb. The approximate area covered by the SMS images used in this study is outlined by the dashed line in the Texas region in the upper left hand panel.

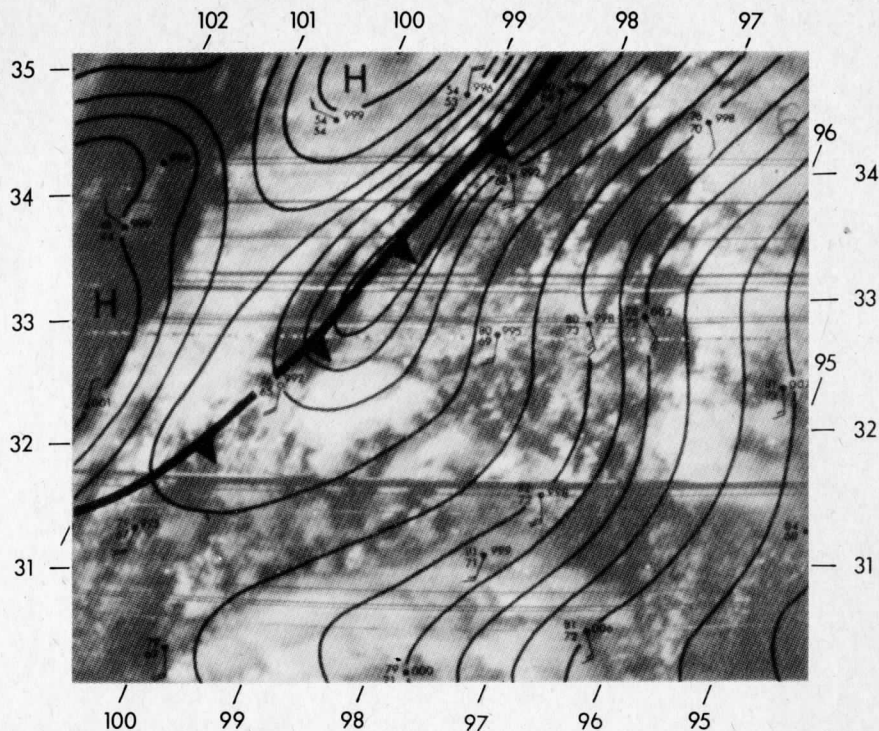


FIG. 3. The surface mesoscale analysis for 1900 GMT on 30 October 1974 for the case study area with the 1902 GMT visible image from SMS superimposed. Contour interval for the surface pressure is 0.02 inch (~ 0.68 mb). Ordinate and abscissa are degrees north latitude and degrees west longitude, respectively.

kinematic method with an adjustment applied to fit boundary conditions. The surface wind divergence field is applied to the layer from the earth's surface to roughly 900 mb in this calculation of vertical motion.

The success of the method depends on limiting the error accrued with each step. In the first step, one obtains numerous vector sequences scattered in the vertical and horizontal. After the editing and time averaging of the second step, these are reduced to single vectors with an rms error estimated in Section 2 to be 4.7 m s^{-1} for the case study to be presented. Step 3, grouping into layers, does not introduce error in itself. Steps 4 and 5 can greatly alter the error characteristics and merit detailed description.

The fourth step, objective analysis, can both introduce and reduce error. Errors are introduced as the vectors are interpolated first linearly to the layer mid-level and then, with a distance-weighted function, to grid points in the plane. The vertical interpolation consists of interpolating each vector vertically to the mid-level according to a linear shear determined for each layer from the Stephenville, Texas, sounding which is assumed, to a crude first approximation, to apply throughout the area of study. At the layer mid-level, horizontal interpolation is accomplished via an outward search from each grid

point for a number n of data points. From these a velocity plane is then constructed by applying a distance-weighted least squares fit to the data. The grid-point value is drawn from the plane constructed. Random error of the cloud motion vectors can be reduced at the grid point if the grid point is surrounded by relatively near data points.

To a first approximation, the reduction in random error from the horizontal objective analysis may be described by the reduction in the standard deviation. The standard deviation of a grid-point value calculated from a linear fit of evenly distributed surrounding n data points with a normal error distribution is

$$\sigma_g = \frac{\sigma_d}{\sqrt{n}}, \quad (1)$$

where σ_d and σ_g are the standard deviations of random error at the data points and grid points, respectively (Hoel, 1954).

For the North Texas case to be discussed, σ_d is 4.7 m s^{-1} and n is 5. An outward search from each grid point of up to 2° was allowed to obtain the five data points. As a first approximation, realizing that vertical interpolation error is not incorporated, the expected random error standard deviation at grid points is then 2.1 m s^{-1} .

Divergence calculations were made using the grid-point wind values. Since the grid points were

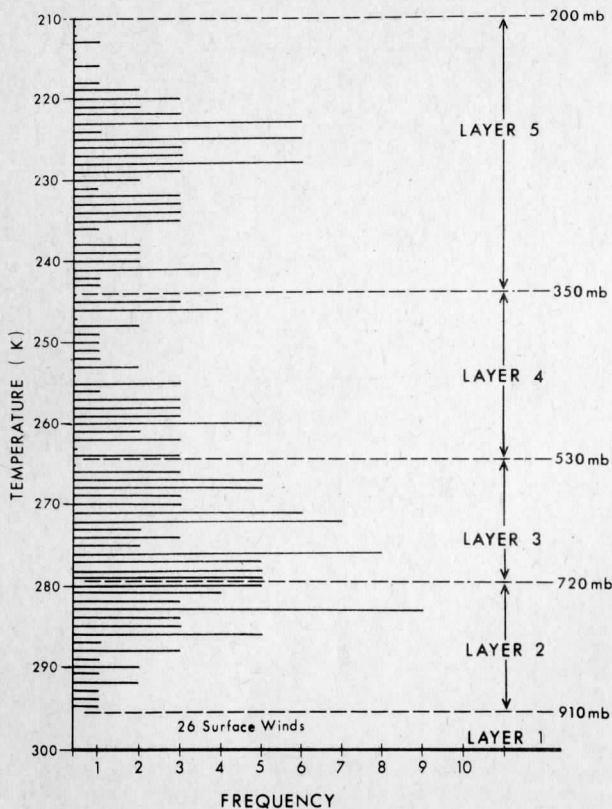


FIG. 4. Vertical distribution of cloud displacement vectors and the limits for layer grouping. Cloud temperature determined from the basic processing procedure is shown on the left-hand ordinate. The approximate equivalent pressures (mb) for the layer bounds are shown on the right hand side.

separated by 50 km, the divergence calculations, obtained from centered differences, are expected to have an error with standard deviation of $\sqrt{2}\sigma_g^2 \div 100 \text{ km} \approx 30 \times 10^{-6} \text{ s}^{-1}$.

From divergence values at all layers and at the earth's surface, vertical motions are calculated via a modified kinematic method (after O'Brien, 1970). If one assumes divergence to be constant throughout a layer of the atmosphere of thickness $p_{n+1} - p_n = \Delta p$, then the vertical motion (omega) at the top of the layer is calculated via the kinematic method to be

$$\left(\frac{dp}{dt}\right)_{n+1} = \left(\frac{dp}{dt}\right)_n - (\nabla_2 \cdot \mathbf{V}_n)\Delta p, \quad (2)$$

where

$\left(\frac{dp}{dt}\right)_{n+1}$ omega at the top of the layer of thickness Δp

$\left(\frac{dp}{dt}\right)_n$ omega at the bottom of the layer of thickness Δp

$\nabla_2 \cdot \mathbf{V}_n$ horizontal divergence within the layer.

The error in divergence calculation is felt to have

increased with height in this test case because of increased velocity errors due to larger wind shears and poorer reliability of cloud tracers at higher altitudes. As a first approximation, a linear increase with height for divergence error is assumed. Accordingly, O'Brien's (1970) modification becomes an adjustment of vertical motions by a second order function in the vertical to fit upper and lower boundary conditions of $dp/dt = 0$ at the earth's surface and at 200 mb for the North Texas case. Just how much error is introduced due to the simplified picture of layer divergences, or how much reduction of error is accomplished by modifying the kinematic method to fit upper and lower boundary conditions is undetermined.

In the North Texas case, the standard deviation of error in divergence calculations was estimated as $30 \times 10^{-6} \text{ s}^{-1}$. A divergence error of this magnitude throughout a constant divergence layer of 190 mb thickness, a typical thickness for this case, introduces an error of $5.7 \times 10^{-3} \text{ mb s}^{-1}$ in omega for the level at the top of that layer. Each layer error is cumulative, so that the total error at any one level reflects the individual errors for that and all lower levels. Errors are muted in the adjustment made for boundary conditions. The adjusted omega values calculated in the North Texas case commonly reach ± 10 to $15 \times 10^{-3} \text{ mb s}^{-1}$, suggesting that the noise or error in the method should not completely mask information about vertical motions.

4. The test case of 30 October 1974

As a first application of our method, satellite imagery of a severe storm outbreak in northern Texas on 30 October 1974 was used. A squall line and severe storm developed on this day in conjunction with a cold front moving swiftly across northern Texas. Although the surface pressure gradients were of only moderate strength, there was pronounced upper air support from a cyclonic system with a closed center as high as 200 mb.

An upper air trough had been moving slowly across the southwest for several days. Such movement of a strong trough out of the deep Southwest is commonly accompanied by severe thunderstorm outbreaks on the plains during the severe weather season. The upper air progression for this case is summarized by the conditions at 200 mb, shown in Fig. 1.

As the upper air trough began moving out of the Southwest, a weak surface low moved from Colorado into southeast New Mexico on the evening of the 29th. Progression of the frontal system across Texas the ensuing day is shown in Fig. 2. During the eastward sweep of the surface front mesoscale thunderstorm activity broke out early. By 1800 GMT two thunderstorm systems had merged into a continuous

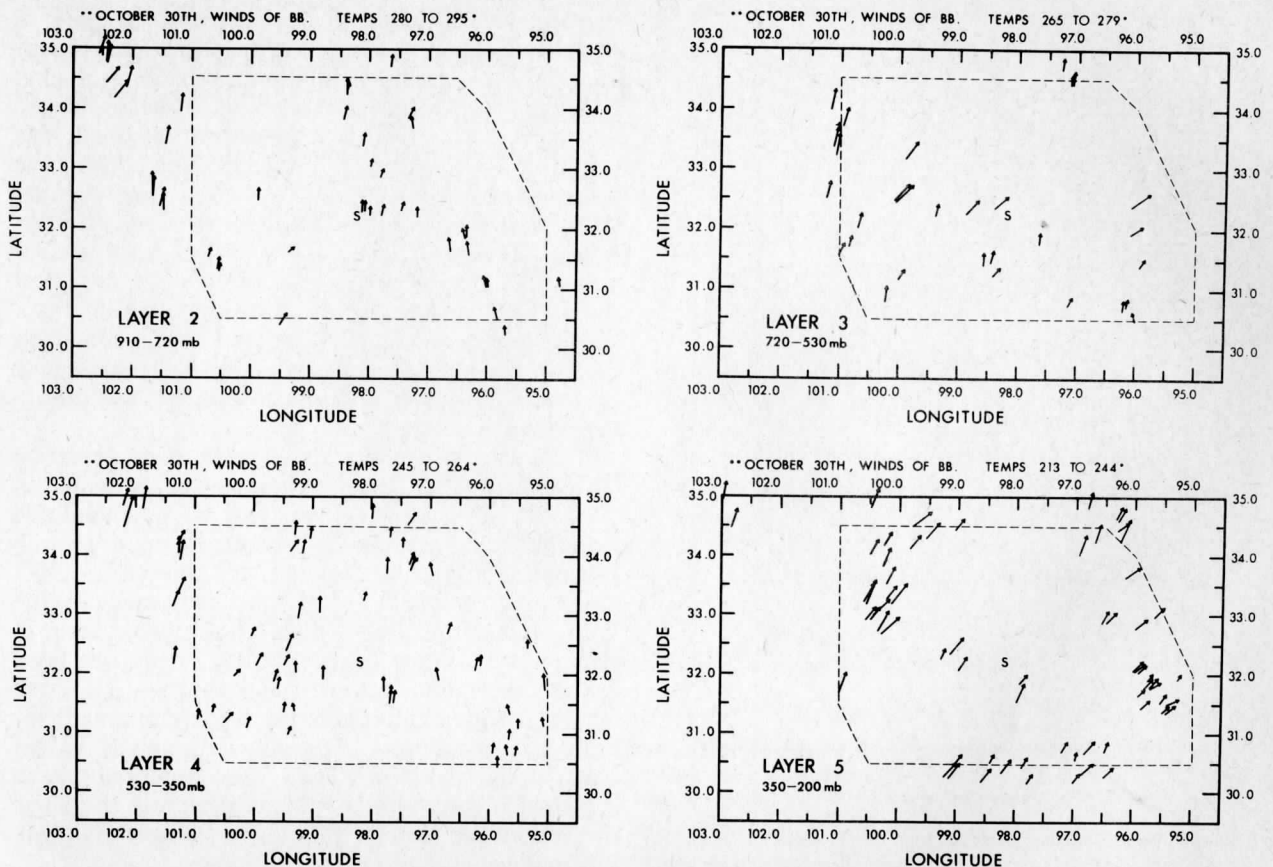


FIG. 5. Horizontal distribution of cloud motion vectors for layers 2 through 5. The length of the arrow is proportional to the speed. The dashed lines outline the area where divergence was determined (see Fig. 7). The position of Stephenville, Texas, is indicated with the symbol S.

line extending across western Texas. By 1900 GMT a mesohigh-mesolow couplet had developed and the cold front position became incorporated with it. This pressure field couplet and the cold front are shown superimposed upon the 1902 GMT satellite image in Fig. 3.

To study the outbreak, five full resolution SMS-1 images of the Texas area were archived at 6 min intervals from 1824 to 1848 GMT. To give perspective on the horizontal scales considered, the approximate area of the SMS images used for analysis is shown on the United States map in Fig. 2. By tracking each selected target through the five images, four sequential cloud motion vectors were constructed during the 24 min tracking time. For convenience, the four vectors for any given target are called herein a "wind series." Targets tracked were primarily such geometric features as cloud centers or edges, typically of two or three pixels (3.0–4.5 km) in diameter. Target lifetimes were generally 18–25 min. A few of the targets were convectively active systems. Although this would be a problem for synoptic-scale data sets, the high density of targets tracked in this mesoscale data set reduces aliasing effects.

Storm outflow properties considered as nonrepresentative motions at the synoptic-scale are representative of mesoscale variations.

In all, 224 wind series were taken. These series were averaged to single vectors and punched onto cards. A manual edit was performed, checking for internal consistency of velocity and emitting temperature calculations of each cloud vector series. Sixteen vector series were eliminated by the edit, leaving 208 for the final set. After considering the Stephenville sounding, it was decided to layer in the vertical as shown in Fig. 4. The vertical distribution of vectors is shown in Fig. 5. Within each layer a representative velocity shear, du/dz and dv/dz , was chosen from the Stephenville soundings of 1200 and 0000 GMT. Fig. 6 depicts the shears chosen. Stephenville's was the only sounding within the area of study and was, fortuitously, located near the area center. No attempt was made to incorporate a number of peripheral soundings to further refine the layering and shear specifications as each reflected upon only a relatively small portion of the area of study.

In the final step gridded values were determined

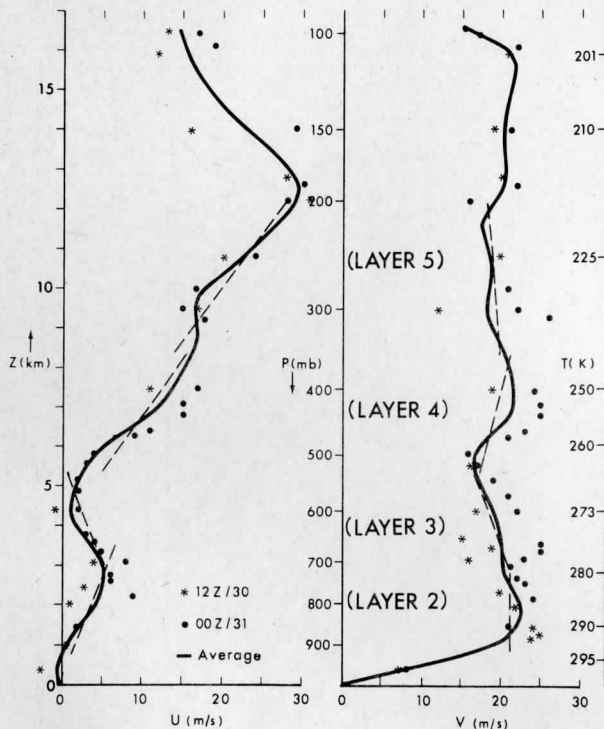


FIG. 6. The Stephenville, Texas velocity component profile for 1200 GMT 30 October and 0000 GMT 31 October 1974. Shears chosen with the layers for the objective analysis are shown by the dashed lines. Labels show the corresponding geopotential, pressure and temperature heights.

and kinematic parameters evaluated. The 208 velocity vectors were objectively interpolated within their respective layers to horizontal grid points at the mid-layers of Fig. 4. The analysis produced gridded fields of horizontal velocity and divergence, from which vertical motions were subsequently calculated. The vertical motions, adjusted to fit upper and lower boundary conditions, are shown in Fig. 7. These are presented in the geographical coordinates of the satellite image used in Fig. 3. Fig. 8 demonstrates the effects of the adjustment needed to set the vertical motion equal to zero at the top of the analysis domain (200 mb). The procedure altered values most strongly at higher levels.

5. Comparative analysis of results

An important output of this work was to determine three-dimensional fields of divergence and vertical motion. Since there were no direct measurements of the actual mesoscale vertical motions over the area of concern and the scale of motions was too small for comparison with the National Meteorological Center models, the calculations were assessed by comparison with surface reports.

Within the region of coverage there were, on the

day of study, eight tornadoes, two severe windstorms, and the surface cold front—all located on Fig. 7. Note that all of the tornadic events occurred some three to six and a half hours after the time of the calculated winds.

Looking at the calculated vertical motions at the top of level 1 (~910 mb) determined from surface wind divergence, one sees that the objective analysis barely suggests upward motion in the cold front area, with little elsewhere. At this level, omega values are calculated from only the surface wind observations, with adjustments for the boundary conditions.

Surprisingly, levels 2 and 3 show a strong pattern of downdraft immediately ahead of the cold front at 720 and 530 mb, with uplift further ahead (SE). The most encouraging result of this work is that all 10 severe storm events occurred in this region of uplift. At the top of level 4, the downdraft-updraft pattern is weakened with the exception of strong uplift at the location of a severe event near 30.7°N, 97.8°W.

The severe weather occurred in regions which were, for the most part, only partially overcast in the satellite images at the time used for this experiment. It should be noted, however, that on this day the atmosphere over the Texas region was convectively unstable. The morning lifted index values ranged from -4.5 at Amarillo to -1.5 at Stephenville, even with morning inversions present, as evidenced by the Stephenville radiosonde soundings. A correlation between regions clear in the morning hours and beset with thunderstorm activity in the afternoon under such unstable conditions has been noted by Weiss and Purdom (1974).

In summary, eight tornadoes occurred within a region which 3-6.5 h prior to the events, was unstable, partially clear, and, according to the calculations presented here, undergoing mesoscale convergence and uplift. It is proposed that the calculated mesoscale uplift, associated with patterns of convergence and divergence, destabilized a large region including the area of severe weather activity. The movement of the surface front into the area of severe weather by 2200 GMT certainly was an additional contributing factor.

6. Conclusions

For the North Texas case presented, the authors developed a three-dimensional, gridded set of wind values via a five-step method. The first step involved obtaining a large set of cloud-displacement vectors. The second and third steps involved quality checking the data and grouping of the data into layers. A key step, the fourth, interpolates data to grid points in a two-segment objective analysis. The final step determines vertical motion from the horizontal motions using a kinematic method. In the North Texas

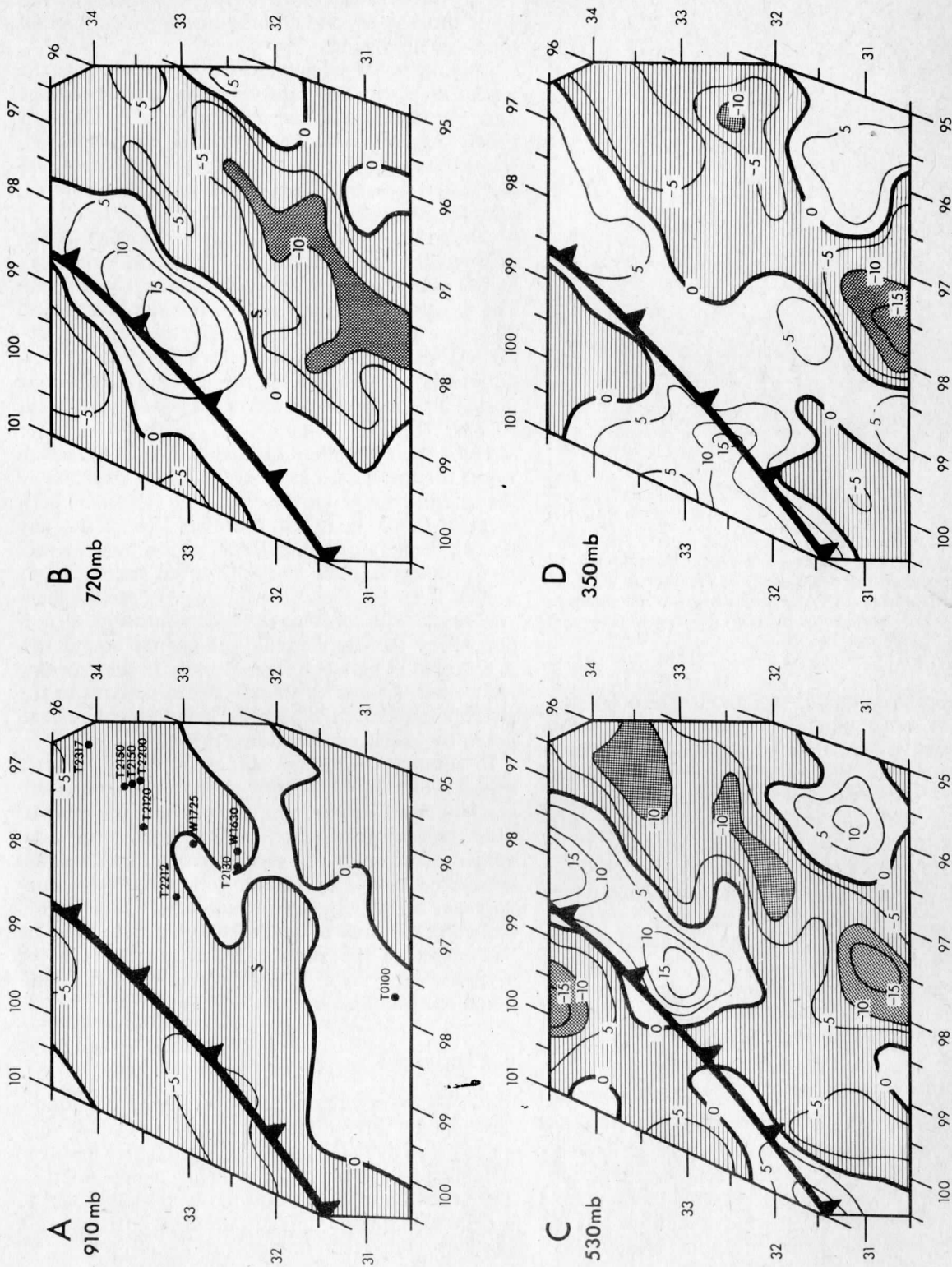


FIG. 7. Adjusted vertical motion, ω ($\times 10^{-3} \text{ mb s}^{-1}$) at the top of layers 1-4 in Panels A, B, C and D (-910 , 720 , 530 and 350 mb), respectively. The position of the surface cold front at 1900 GMT is shown on all panels. The location and GMT times of severe weather events on the day of study is shown in Panel A using W and T to denote windstorm and tornado respectively. Contour interval is $5 \times 10^{-3} \text{ mb s}^{-1}$. Shading indicates the areas where motion is upward. The heavier shading is for magnitudes $> 10 \times 10^{-3} \text{ mb s}^{-1}$. Ordinate and abscissa are degrees north latitude and degrees west longitude, respectively. The position of Stephenville, Texas, is indicated in Panels A and B with the symbol S.

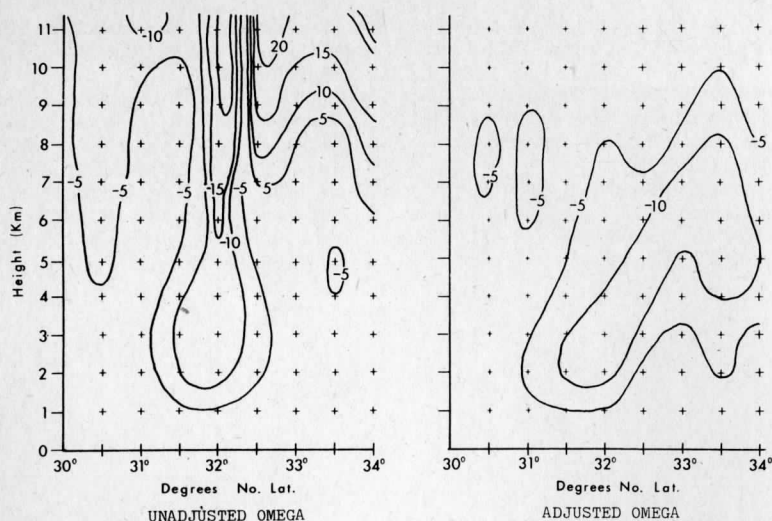


FIG. 8. Vertical cross section for vertical motion, omega ($\times 10^{-3}$ mb s^{-1}), along the 96° W longitude. The original and adjusted data are shown to illustrate the effects of the adjustment procedure.

case, the standard deviation of the magnitude of the vector error at the grid points has been estimated as 4.7 m s^{-1} . Consequently, the standard deviation of error in divergence calculations is $30 \times 10^{-6} \text{ s}^{-1}$, and this error results in standard deviation of error in vertical motion calculations from a typical layer of $5.7 \times 10^{-3} \text{ mb s}^{-1}$. Values of omega calculated in the North Texas case often reached ± 10 to $15 \times 10^{-3} \text{ mb s}^{-1}$.

The results were consistent with other features of the situation. The satellite data gave a strong pattern of downdraft immediately ahead of the cold front from ~ 910 to 530 mb , with uplift further ahead from 910 to 350 mb . All eight reported tornadoes within the area of coverage on 30 October occurred within this region of uplift. At the time of the calculations (1824–1848 GMT) skies over the region of downdraft were primarily clear, with some broken overcast. The axis of calculated uplift further east spanned from thunderstorms in the northeast southwestward through a mix of clear skies and small-scale convection. The tornadoes were first noted in the western edge of the region of calculated uplift and subsequently reported at locations further east and northeast. It is proposed that mesoscale uplift, associated with patterns of convergence and divergence measured by the authors, destabilized a large region including the area of severe weather activity. It is encouraging that the satellite cloud wind data appears to have provided reasonable and useful information for mesoscale wind fields in the atmosphere.

Acknowledgments. Thanks are extended to many persons in the Space Science and Engineering Cen-

ter for assistance with various parts of this research. Fred Mosher, John Benson, J. T. Young, Gary Chatters and Ken Yuen need especially to be recognized for their help. Profs. Lyle Horn and Eberhard Wahl in the Meteorology Department are also thanked for their assistance. The anonymous reviewers helped greatly to improve the clarity of the paper with their constructive comments.

This work was supported by the National Science Foundation under Grants ATM 75-03617 and ATM 77-20231.

REFERENCES

- Bauer, K. G., 1976: A comparison of cloud motion winds with coinciding radiosonde winds. *Mon. Wea. Rev.*, **104**, 922–931.
- Bengtsson, L., 1975: Four dimensional assimilation of meteorological observations. GARP Publ. Ser., No. 15, WMO, 76 pp.
- Hasler, A. E., W. E. Shenk and W. C. Skillman, 1977: Wind estimates from cloud motion: Results from Phases I, II, and III of an *in situ* aircraft verification experiment. *J. Appl. Meteor.*, **16**, 812–815.
- Hoel, P. G., 1954: *Introduction to Mathematical Statistics*, 2nd ed. Wiley, 331 pp.
- Hubert, L. F., and L. F. Whitney, Jr., 1971: Wind estimation from geostationary satellite pictures. *Mon. Wea. Rev.*, **99**, 665–672.
- Mosher, F. R., and B. Sawyer, 1976: Comparison of wind measurement systems: cloud tracked winds vs. rawinsonde winds and rawinsonde winds vs. rawinsonde winds, Section II, GISS/SSEC McIDAS data study. Final Tech. Rep. Contract NGR 50-002-215 for the period 1 March 1973–31 May 1976, Space Science and Engineering Center, University of Wisconsin, Madison.
- O'Brien, J. J., 1970: Alternative solutions to the classical vertical velocity problem. *J. Appl. Meteor.*, **9**, 197–203.
- Reiter, E. R., 1961: *Jet Stream Meteorology*. The University of Chicago Press, Chicago, 515 pp. [English Translation, 1963].

- Suchman, D., and D. W. Martin, 1976: Wind sets from SMS: An assessment of quality for GATE. *J. Appl. Meteor.*, **15**, 1265-1278.
- Suomi, V., 1975: Man-Computer Interactive Data Access System (McIDAS). Final Rep. Contract NAS5-23296 for Goddard Space Flight Center, Space Science and Engineering Center, University of Wisconsin, 254 pp.
- U.S. Air Force, 1963: Meteorological Handbook, AFMTCP 105. Air Force Missile Test Center, Patrick AFB, FL, 12 pp. [Available from Tech. Publ., Detachment 1, SAMTEC, Patrick Air Force Base, FL 32925]
- Weiss, C. E., and J. F. W. Purdom, 1974: The effect of early-morning cloudiness on squall-line activity. *Mon. Wea. Rev.*, **102**, 400-402.
- Wiegman, E. J., R. H. Blackmer, S. M. Serebreny and S. M. Hadfield, 1971: Analysis of ATS-1 photographs using a specially designed electronic console. Stanford Res. Center, Contract NAS5-21086 to NASA-GSFC. [NTIS N71-31421].
- Wilson, T. A., 1976: The determination of mesoscale horizontal and vertical wind fields from SMS-1 satellite observations. Master's thesis, Dept. of Meteorology, University of Wisconsin, Madison, 124 pp.

NUMERICAL MODEL INITIALIZATION WITH SUBSYNOPTIC-SCALE
SATELLITE CLOUD-WIND DATA

David D. Houghton and Dong K. Lee

Department of Meteorology
University of Wisconsin
Madison, Wisconsin

and

Chia-Bo Chang

Department of Physics and Atmospheric Science
Drexel University
Philadelphia, Pennsylvania

1. INTRODUCTION

Realization of the full potential value of subsynoptic-scale wind data derived from satellite images (hereafter referred to as satellite winds) depends strongly on the use of regional mesoscale numerical models. The numerical models are required to effect merging of this data with other forms in a compatible manner as well as to demonstrate impacts and advantages for the description and prediction of the state of the atmosphere.

Subsynoptic-scale satellite wind data sets have become available in the last few years in sufficient numbers and with adequate quality control to justify preliminary experimentation with numerical models. Many papers given at the AMS Tenth Conference on Severe Local Storms in Omaha, Nebraska, October, 1977 showed such satellite-wind sets. Preliminary estimates of data quality have been made by Suchman and Martin (1976), Hasler, Shenk and Skillman (1977) and Wilson and Houghton (1979) to name a few. Additional judgements on quality await further compatibility tests that numerical model experimentation will provide.

Model initialization embodies the key problems associated with employing any data type in a numerical model: The first step requires interpolating data point information to the grid point positions in the model. This is a critical and nontrivial task for data sets as irregular as the satellite wind data. The second step involves achieving a compatibility between the particular data form and all the other variables in the model. Such compatibility is evaluated by smoothness of fields, diagnostic relationships and evolution (adjustment) in the beginning stages of a numerical simulation. In this study both of these aspects of initialization are considered for a middle latitude subsynoptic scale satellite-wind data set obtained for May 20, 1977 over the Central United States.

2. DESCRIPTION OF BASIC DATA

The satellite-wind data used in this study

are 18-minute averaged wind vectors obtained from four SMS images of 6-minute interval from 1742 to 1800 GMT on May 20, 1977 in the Kansas, Oklahoma and western Missouri area. Fig. 1 shows the high resolution SMS visible image for 1742 GMT. The data set was produced using single pixel tracking technique on the McIDAS developed by the Space Science and Engineering Center at the University of Wisconsin. Some wind vectors in the data set were eliminated after they were tested under quality control and the few vectors at middle and high levels were too sparse to be considered in this study. The final data set consisted of 180 low level wind vectors as shown in Fig. 2.

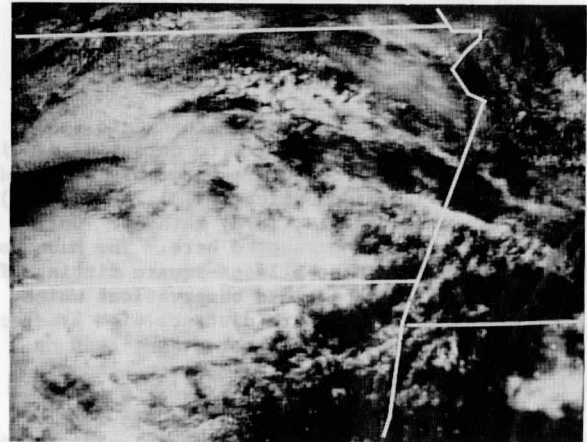


Fig. 1. High resolution visible SMS image for 1742 GMT 20 May 1977 over Kansas and smaller sections of Missouri, Oklahoma, Nebraska and Arkansas. State boundaries are shown by white lines.

Most of target clouds are low level cumulus with top heights ranging approximately from 750 mb to 850 mb. In the southwestern quarter of the area, there was extensive cumulus cloud coverage (see Fig. 1) which reduced the number of satellite wind vectors that could be obtained in that area. The cloud elements in the northeastern corner (shown as E in Fig. 2) have relatively short life

spans and less satisfactory tracking characteristics than elsewhere.

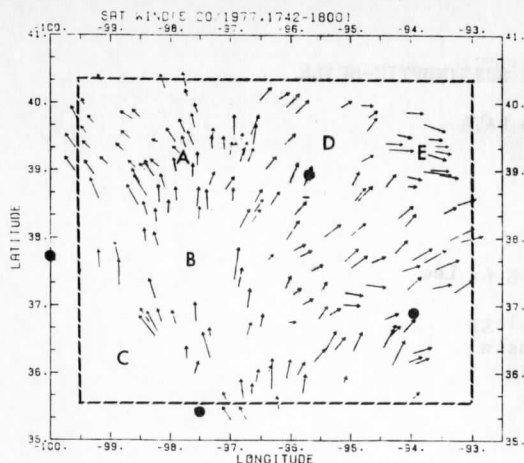


Fig. 2. Original low-level satellite-wind data set obtained for the study area from 1742-1800 GMT SMS images. The length of the vector is proportional to wind speed. The locations of the four upper air stations in the region are shown by the dots. The letter symbols identify areas of specific interest as follows: A, data dense area; B, C and D, data sparse areas; E, area with short-lived cloud tracers.

The synoptic situation at this time shows a broad area of low level southerly wind flow into the region of interest. By 0000 GMT May 21, the southerly winds had increased and a strong thunderstorm band existed through central Oklahoma, Kansas and Nebraska. In the area studied, the middle and upper level winds are diffluent and generally southwesterly with speeds decreasing along the streamlines going towards the northeast.

3. APPLICATION OF OBJECTIVE ANALYSIS TO SATELLITE DATA

3.1 Description of Methods

Four objective analysis methods are tested on the satellite-wind data set to determine sensitivity to analysis procedure. These are referred to as the Mancuso and Endlich (1973), MACC (1978), Gandin (1963) and Barnes (1973) methods. Only a brief description is presented here. The Mancuso and Endlich method uses a least-square fitting of a first-degree polynomial to observations which are weighted inversely with distance with greater weighting to along-stream observations than to cross-stream data. The MACC (Madison Academic Computing Center) method is a general mathematical procedure which uses a least-square fitting of a quadratic polynomial to observations and then applies a smoother to the interpolated grid values. The Gandin method incorporates a minimization procedure for root mean square error in the determination of grid point values from station values. For this method an exponential function which decreases with distance is chosen to represent covariances because the mesoscale characteristics of the covariances are still unknown. In this formulation of Gandin's method, the linear equation system solved for optimal weights tends to have a quasi-singular matrix when observations are very close to each other. The data set in this study has many close observations and it is

necessary to replace individual values by an averaged value of observations within a certain distance to make the analysis procedure work. The Barnes method obtains interpolated values at grid points from observations using a weighting factor that is a function of distance and a function of data distribution characteristics. In a second pass the interpolated field is made to converge to observed values by including a weighted correction-field effect in the specification of the weighting factor. This method has the advantage of being able to filter the noise levels without changing the weight functions.

Each method is used to determine grid point values of velocity on a 35 km grid mesh in the domain outlined by the dashed line in Fig. 2. Basic characteristics and specific parameter specifications of the methods used in this study are summarized in Table 1.

3.2 Results

All methods show generally similar phase relationships of both divergence and vorticity. Typical magnitudes are $5 \times 10^{-5} \text{ s}^{-1}$ for both vorticity and divergence. In the Mancuso and Endlich, MACC and Barnes methods 6Δ wavelengths (210 km) are dominant while in the Gandin method 4Δ wavelengths (140 km) seem to be more dominant (where Δ = grid spacing). Thus all methods are able to provide subsynoptic scale features. Dominance of positive divergence and anticyclonic vorticity throughout the region are indicative of synoptic-scale features that exist along with the subsynoptic scale phenomena.

Fig. 3 shows the divergence fields computed by the four methods. Maximum and minimum values of the four methods are generally very comparable to each other; although in the Gandin method, some of the extrema values are much larger than those of the other methods. In the data-sparse region (shown as B in Fig. 2), large amplitude differences and phase shifts of the divergence field exists between the methods.

The differences in divergence between the Barnes and the other three methods, respectively, are shown in Fig. 4. In each case, the Barnes method results have been subtracted from the other method. Typical magnitude of differences in divergences is half that of divergence values except in the comparison of the Barnes and Gandin methods. These difference values are relatively small in the data-dense region (shown as A in Fig. 2) but large in the data-sparse regions (shown as B, C and D in Fig. 2). These difference maps do not determine which method gives the best correspondence to the observed data. It is, nevertheless, obvious that the Gandin method is less consistent with the other methods and therefore probably is not as satisfactory for interpolating grid fields for this satellite-wind data set.

Fig. 5 shows the vorticity fields computed by the Mancuso and Endlich and Barnes methods. Significant differences between the two methods are indicated in the extrema values in the data-sparse region (B in Fig. 2) even though the patterns agree very well to each other. This clearly demonstrates that gridded data sets obtained from data containing large spatial variations in density is strongly dependent upon the method used.

Table 1. Comparisons of basic characteristics and parameter specifications of objective analysis methods used in this study. Symbols are defined as follows: Δ is the grid spacing, \bar{R} is a normalized distance between grid point and data point, and C_1 , C_2 and C_3 are non-dimensional coefficients. The cpu time includes computation of divergence and vorticity.

	Mancuso and Endlich	MACC	Gandin	Barnes
Number of observations used to interpolate one grid value	up to 8	8	8	dependent on data density
Search radius from a grid point	2Δ	dependent on data density	dependent on data density	dependent on data density ($\approx 4\Delta$)
Weighting Factor	3 coefficients of 1st degree polynomial and $\frac{1}{1+[\bar{R}+ \bar{R}_x\bar{V}]^2}$	6 coefficients of quadratic polynomial	$\exp(-C_1 \bar{R} ^2)$	$\exp(-C_2 \bar{R} ^2)$ for 1st pass $\exp(-.3C_3 \bar{R} ^2)$ for 2nd pass
Smoothing	no	yes	averaging for very close data points (within 1Δ)	no
cpu time for case study (s)	20.886	19.476	16.771	33.053

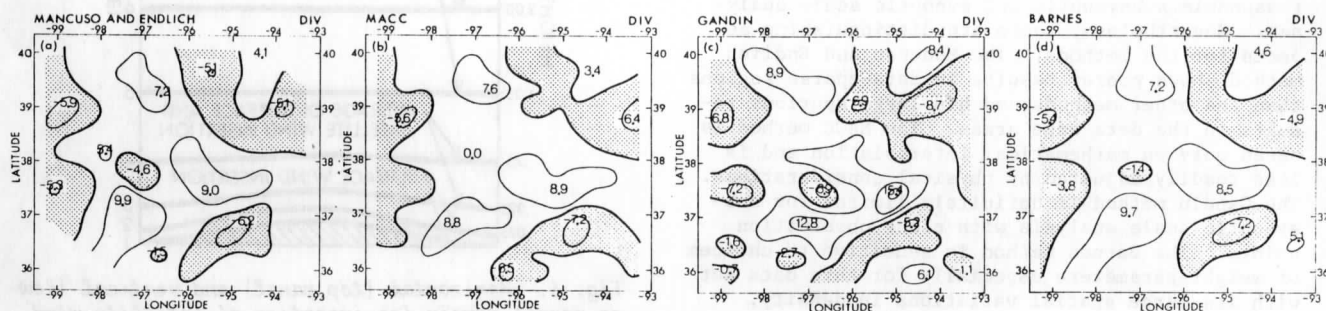


Fig. 3. Divergence ($10^{-5} s^{-1}$) computed from gridded data determined by the Mancuso and Endlich, MACC, Gandin and Barnes objective analysis methods in panels a, b, c and d respectively. The thick solid lines are zero contours and contour interval is $5 \times 10^{-5} s^{-1}$. Shading indicates regions of negative divergence (convergence). The numbers indicate the position and value of local extrema. Contours are omitted in all corners except the upper left in the analysis from the Mancuso and Endlich method due to exceptionally spurious edge effects.

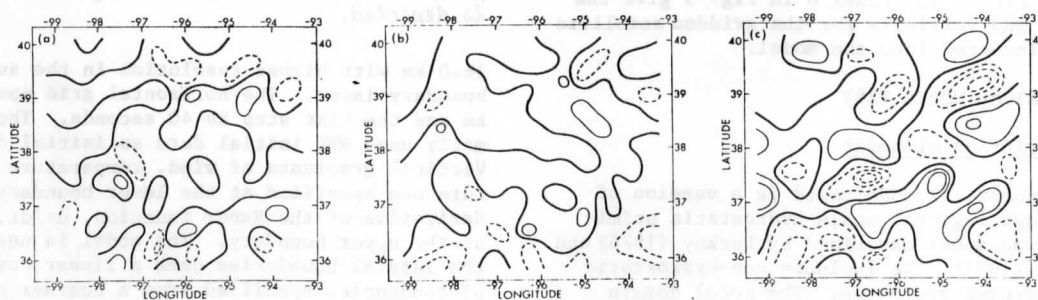


Fig. 4. Difference in divergence ($10^{-5} s^{-1}$) between the Barnes method results and the Mancuso and Endlich, MACC and Gandin method results in panels a, b and c respectively. In each case the Barnes values are subtracted from the other values. The thick solid lines are zero contours; the thin solid lines are positive value contours; and the thin dashed lines are negative value contours. Contour interval is $2.5 \times 10^{-5} s^{-1}$. Contours are omitted in all corners except the upper left in the analysis from the Mancuso and Endlich method due to exceptionally spurious edge effects.

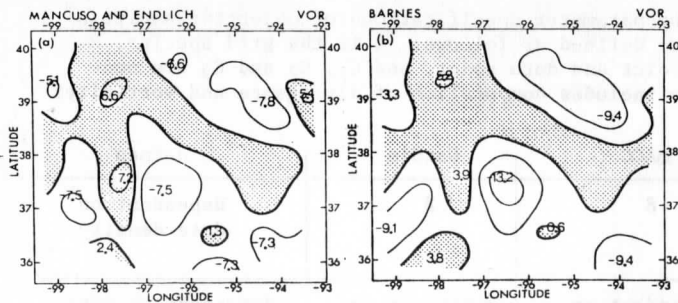


Fig. 5. Vorticity ($10^{-5} s^{-1}$) computed from gridded data determined by the Mancuso and Endlich and Barnes objective analysis methods in panels a and b respectively. Contour interval is $5 \times 10^{-5} s^{-1}$. Shading indicates regions of positive (cyclonic) vorticity. The numbers indicate the position and value of local extrema. Contours are omitted in all corners except the upper left in the analysis from the Mancuso and Endlich method due to exceptionally spurious edge effects.

For this test analysis the Barnes, Mancuso and Endlich and MACC methods generally agree well with each other for amplitudes and patterns of both divergence and vorticity, whereas the Gandin method does not show good agreement to the others in terms of magnitude. All methods greatly suppress 2Δ features (70 km wavelength) and provide reasonable subsynoptic and synoptic scale analyses. Nevertheless, there are distinguishing aspects for the methods. The Mancuso and Endlich method shows poorer results in data-sparse regions than the other methods and has large spurious results in the data edge areas. The MACC method is based only on mathematical interpolation and is less readily adjusted by physical considerations. The Gandin method is definitely limited for subsynoptic scale analysis with close observation points. The Barnes method is sensitive to choices of weight parameters especially for this data set with its large spatial variations in density.

The Barnes method was selected to provide the grid point wind data set for initialization of the numerical model in this study. Its sensitivity to choice of weighting parameters made it possible to obtain dimensions and amplitudes of the subsynoptic scale features consistent with those developed normally by the numerical model. Panel d in Fig. 3 and Panel b in Fig. 5 give the divergence and vorticity for the gridded satellite wind data inserted into the model.

4. NUMERICAL MODEL TEST

4.1 Description of model

The numerical model used is a version of the fine mesh regional scale hydrostatic primitive equation model described by Perkey (1976) and Kreitzberg (1977). It includes non-hydrostatic moist convective processes. The model domain ranges from (north) latitudes 30° to 45° and from (west) longitudes -104° to -86.6° . The model uses height above surface terrain as the vertical coordinates and Cartesian coordinates in the horizontal. The lower boundary is terrain following with a gradual reduction of the coordinate distortion with height. It has 15 levels from 0 to

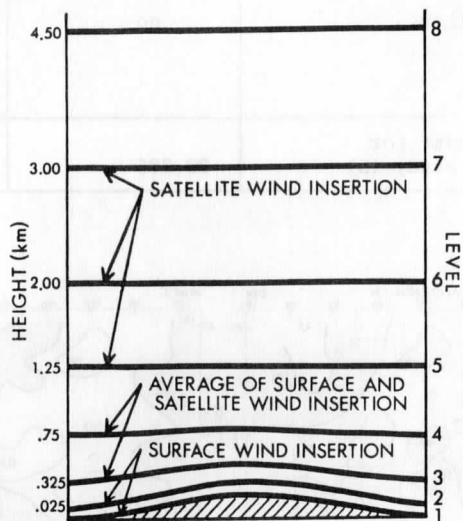
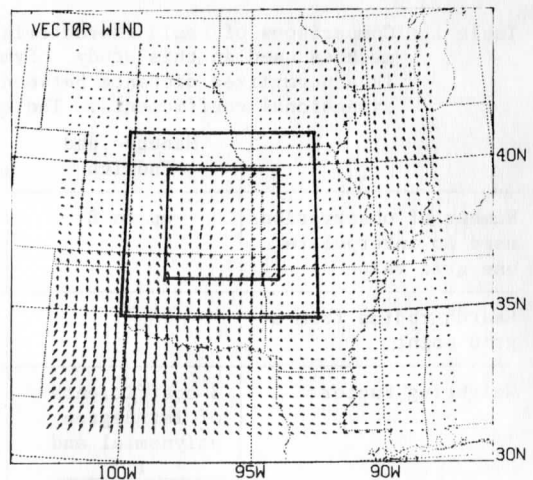


Fig. 6. Horizontal (top panel) and vertical (lower panel) domain for insertion of satellite-wind data into the numerical model. In the top panel the inner rectangle is part of the insertion area where no boundary smoothing is done. The transition boundary zone is between the two rectangles. The plotted wind vectors which show the grid resolution and model domain are for unsmoothed initial data in the insertion experiment. In the lower panel, only the lower portion of the 15 layer model is depicted.

16.0 km with higher resolution in the surface boundary layer. The horizontal grid spacing is 35 km and the time step is 40 seconds. The model normally uses NMC initial data as initial conditions. Vertical gradients of wind, temperature and moisture are specified at the lower boundary and the derivative of the Exner function, $d\pi/dt$, is zero at the upper boundary. The model is nested and at the lateral boundaries uses a linear combination of tendencies specified from a coarser mesh model simulation and tendencies calculated by the model.

4.2 Experimental design

Two 6-hour simulations starting from 1800 GMT 20 May 1977 are made with the numerical model. The first, referred to as the "Control" case is

initialized from 6 hour forecast fields from a coarser mesh model run that used 1200 GMT rawinsonde information as input. The second, referred to as the "Insertion" case, is handled identically to the first except for the initial time insertion of satellite-wind data into a sub-domain of the model without any modification of the mass and pressure fields. Comparison of the two simulations delineates the impact of the satellite-wind information.

Fig. 6 shows the domain of insertion in terms of vertical and horizontal grid resolution. For the insertion case, surface hourly wind observations at 1800 GMT replace the model winds at levels 1 and 2, satellite-wind data replace the model winds at levels 5, 6 and 7, and averaged values of surface and satellite-wind data replace the model winds at level 3 and 4 in the insertion area. Levels 5-7 correspond closely to the 900-700 mb height layer originally assigned to the satellite-wind vectors. There are strong discontinuities in the wind fields at the insertion boundaries, in particular, northern and eastern boundaries. A special transition boundary zone is used to smooth these discontinuities as shown in Fig. 6. It is a band 4 grid increments wide surrounding the insertion area and consists of one grid row at the edge of the insertion area and three grid rows outside the area. The grid point values in the transition boundary zone are recomputed by a linear interpolation of the satellite-wind data one grid distance inside the insertion domain and model winds 4 grid spacings outside the insertion domain.

After all initial data has been assembled in the model, an adjustment is made in the horizontal velocity field so that the vertical motion is zero at the upper boundary. This minimizes the initial excitation of spurious external wave modes. This is done by an iterative procedure making corrections at all levels and is applied to the entire model domain including the region where satellite wind data has been added in the Insertion case. In the insertion region the adjustment procedure suppresses slightly amplitudes of divergence in the satellite-wind data but it does not effect the phase and patterns of the small scale features. At upper levels it results in adding divergence of opposite sign to that in the satellite wind data at lower levels.

Fig. 7 shows the resultant initial time values of divergence and vorticity at the 2 km level (approximately 800 mb) in the Control and Insertion cases. (Note the coordinate height is

not exactly 2 km due to terrain effects but it is very close in the insertion region.) The 2 km level is in the middle of the three levels where satellite-wind data was added. For reference the region where the satellite data was inserted including the transition boundary zone is shown.

4.3. Results

Fig. 8 shows the predicted 2 km level divergence and vorticity fields after 1 hr in the Control and Insertion cases. The amplitudes of the divergence fields in the satellite wind data area are considerably reduced to less than 40% of initial values. Nevertheless, the patterns and phase relationships of divergence remain consistent with the initial state. Significant divergence develops in the transition boundary zone by 1 h with magnitudes similar to, but not exceeding those in the interior. The divergence that develops at higher levels (7.5 km and above) is generally of opposite sign but with similar magnitudes to those at lower levels indicating the presence of internal mode structure in the subsynoptic scale features introduced from the satellite-wind data insertion. In the insertion area there is no rapid oscillation dominating the divergence field. The convergence area in the SE corner moves gradually to the north in the 1, 2, 3 and 6 h difference maps. Divergence in the western part changes to convergence in some areas but only after 6 h.

It is important that the signal and noise generated by the insertion correspond to internal mode structure so that horizontal propagation speeds are low and constraints of the limited dimensions in the horizontal domain do not result in an obscuration of the simulation by boundary effects. Judging by the difference maps up to 6 h, the outward (and probably inward) propagation speed of the noise structures produced in the transition boundary zone is about 30 m s^{-1} which means that the effects do not reach the model boundaries until around 6 h.

The model results and case differences after 6 h for divergence and vorticity at 2 km are shown in Fig. 9. The difference map for divergence shows larger values than at 1 h in the insertion area and the remnants of some of the initial patterns are still present demonstrating that the model has captured slow moving components in the cloud-wind divergence fields which could correspond to physically realistic patterns. The difference map also shows the spread of the satellite-wind divergence effects to the model boundaries particularly along a NE-SW axis which approximate the direction of flow at upper tropospheric levels.

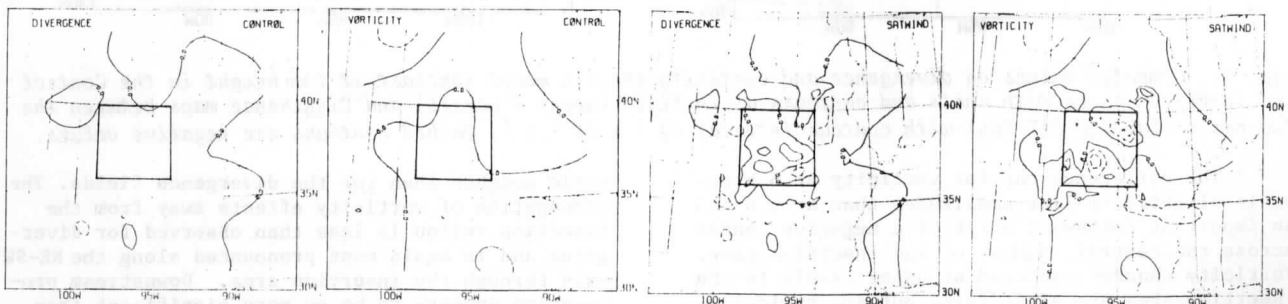


Fig. 7. Initial time (1800 GMT) values for divergence and vorticity at 2 km height (approximately 800 mb) in the Control and Insertion (labeled SATWIND) cases. Units are 10^{-5} s^{-1} . Contour interval is $5 \times 10^{-5} \text{ s}^{-1}$. Dashed contours are negative values. The insertion area is shown here (and in subsequent Figs.).

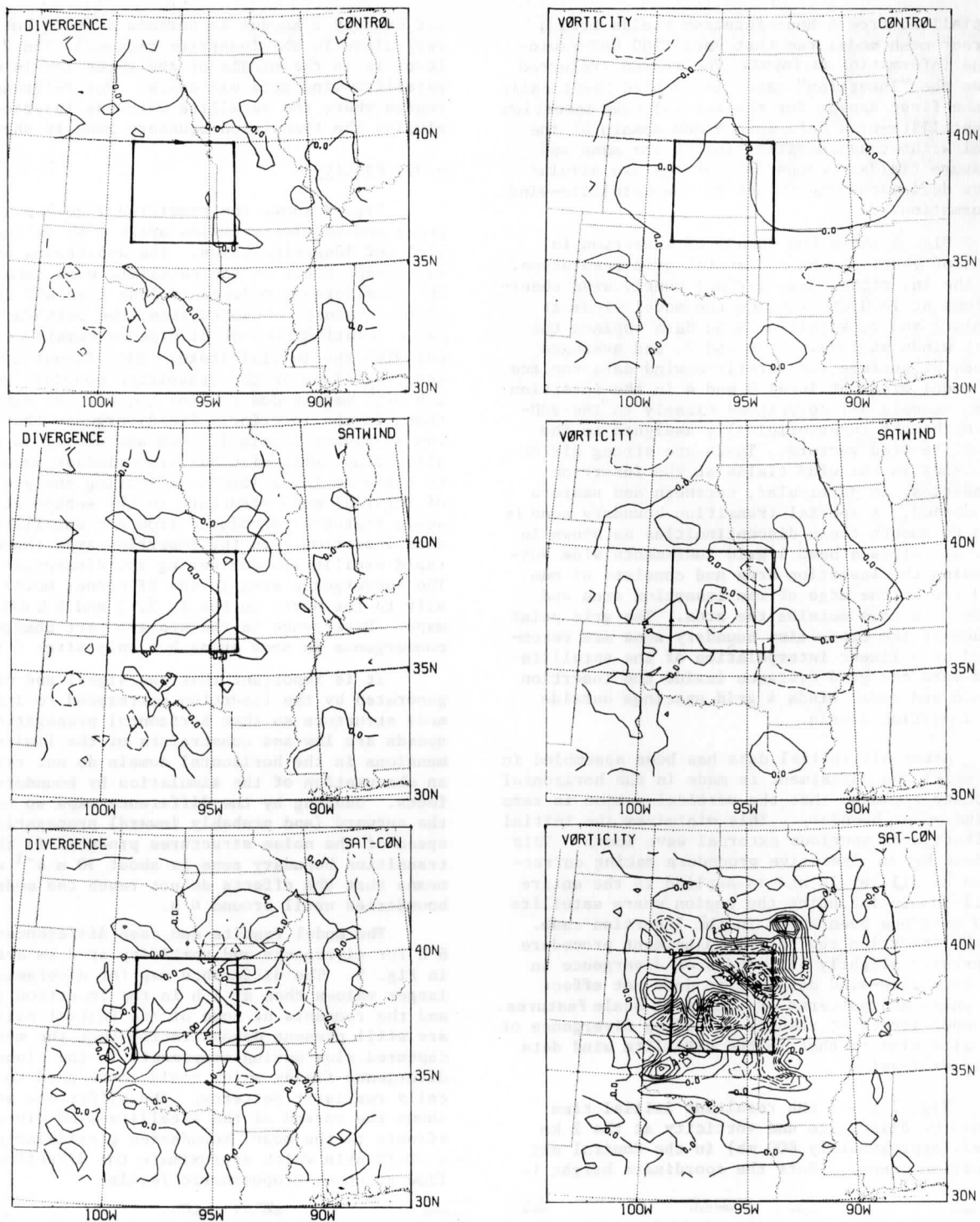


Fig. 8. Computed values of divergence and vorticity for 1 h model forecast at 2 km height in the Control and Insertion cases with units and contours as in Fig. 7 (upper 4 panels) and Difference maps between the two cases (labeled SAT-CON) with contour interval of $1 \times 10^{-5} \text{ s}^{-1}$. Dashed contours are negative values.

The difference map for vorticity at 6 h reveals slightly smaller amplitudes than at 1 h and an important northward shift of a negative center across the central region of the insertion case. Vorticity changes produced at upper levels in the insertion area are significant but are typically less than half the magnitude of those at lower levels. There appears to be a general agreement in sign between these levels indicating deeper

scale heights than for the divergence fields. The propagation of vorticity effects away from the insertion region is less than observed for divergence and is again most pronounced along the NE-SW axis through the insertion area. Downstream propagation appears to be no more significant than upstream propagation.

General effects of the data insertion on

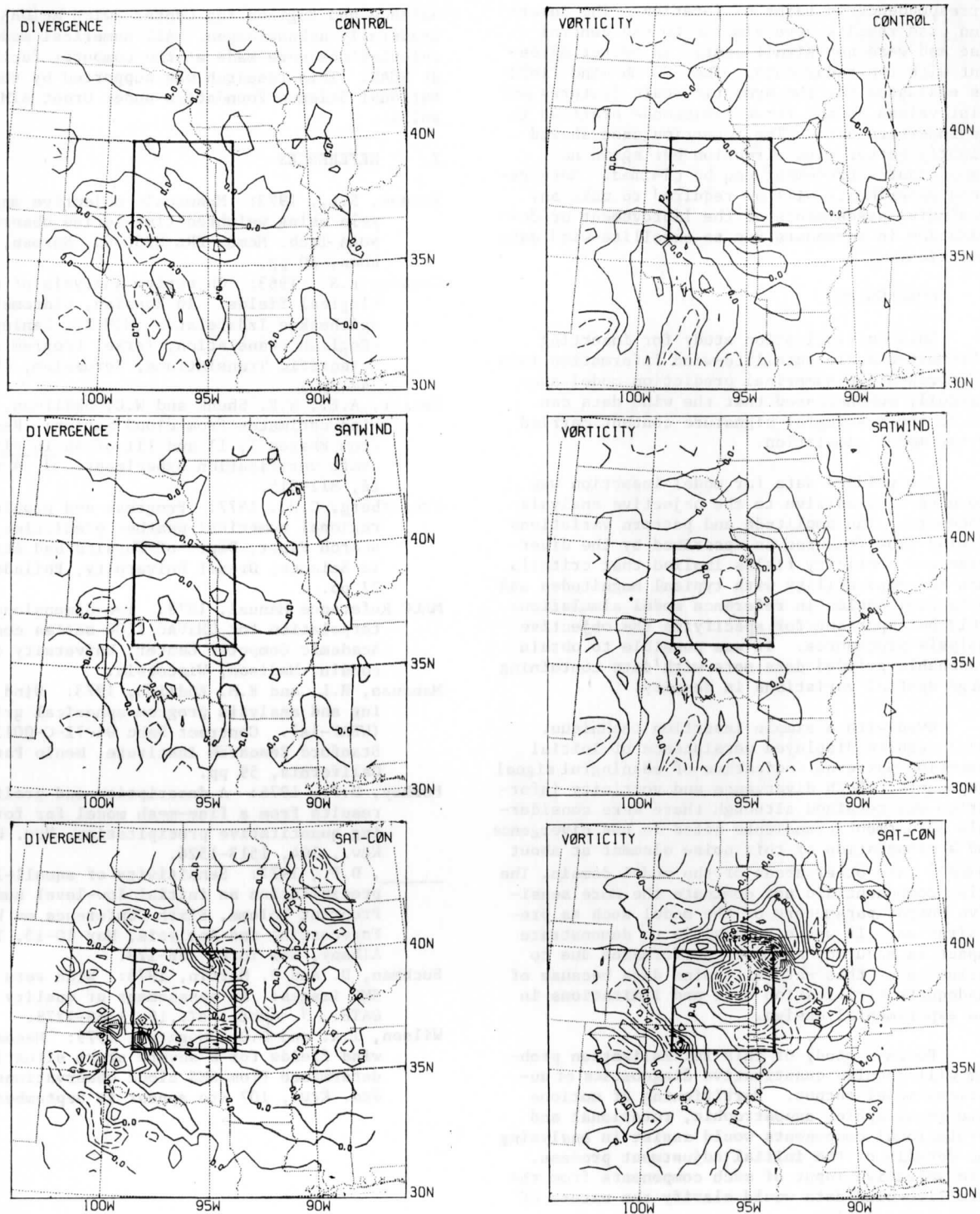


Fig. 9. Same as Fig. 8 except for 6 h model forecasts.

precipitation forecasts (one of the most sensitive output parameters) was examined. There is little difference in the 6 h accumulated precipitation forecast between the two cases. Perhaps a longer forecast would show more effects of the insertion. Perkey (1977) used 18 h model results to demonstrate precipitation forecast sensitivity to the initial moisture specification.

A brief comparison of model results with observational data was made to see if the impact of

the satellite-wind data on the model forecast was favorable, i.e. if the model results correspond more closely to the verification with the additional initialization data. Unfortunately, the resolution in the observations is not sufficient to make many meaningful verification evaluations of the subsynoptic scale features in the model forecasts. Two parameters were considered, precipitation and 700 mb winds. Forecast convective precipitation rates were compared with NWS Fax radar depictions of convection to determine

correspondence in terms of location. The insertion case results were similar to the control case and were not significantly in better agreement with the radar data. The 700 mb wind field was evaluated for the synoptic scale features and point values at the three rawinsonde stations in the insertion area. The insertion case showed slightly better wind direction but again no significant improvement can be claimed. More refined experiments will be required to make any meaningful assessments of the improvement or degradation in forecasts due to satellite-wind data insertion.

5. CONCLUSIONS

This initialization study for inserting subsynoptic scale satellite-wind information into a comprehensive numerical prediction model successfully demonstrated that the wind data can add to the meaningful signature content carried by the model simulation.

The gridded data for model insertion was shown to be sensitive to the objective analysis procedure. The amplitude and pattern variations of wind flow features as described by the divergence and vorticity fields implied that criteria such as comparability with typical magnitudes and horizontal scales in reference model simulations would be important for specifying the objective analysis procedures. It was possible to obtain reasonable gridded data sets with data containing large spatial variations in density.

Even with a simple insertion technique, model results displayed persistence of initial insertion patterns indicative of meaningful signal components. Both divergence and vorticity information was retained although there were considerable adjustment transients noted in the divergence and a propagation of this noise element at about 30 ms^{-1} into other areas of the model domain. The noise component did not dominate the more sensitive output parameters of the model such as precipitation. It was not possible to demonstrate impact in accuracy of model performance due to inclusion of this satellite-wind data because of inadequate verification data and limitations in the experimental design.

Further study of this initialization problem will require quantitative diagnostics of numerical model output. Partitioning of motions into geostrophic, ageostrophic, rotational and irrotational components would assist in analysing the details of the initial adjustment process. More selective input of such components from the satellite-wind data would clarify the nature of model assimilation.

6. ACKNOWLEDGEMENTS

The authors are grateful to Dr. Carl W. Kreitzberg at Drexel University and Dr. Donald J. Perkey and other staff in the Joint Project between Drexel's Atmospheric Sensing and Prediction Project and NCAR's Mesoscale Research Project (at NCAR) for helping with the Drexel-NCAR regional scale numerical model. We also thank Mr. Peter Guetter and Mr. Thomas Whittaker both of the University of Wisconsin for computing assistance. The assistance of staff in the Space

Science and Engineering Center with McIDAS is gratefully acknowledged. All numerical model calculations were made at the computer facility at NCAR. This research was supported by the National Science Foundation under Grant ATM77-20231.

7. REFERENCES

- Barnes, S.L., 1973: Mesoscale objective map analysis using weighted time-series observations, NOAA Tech. Memo. ERL NSSL-62, Norman, Oklahoma, 60 pp.
- Gandin, L.S., 1963: Objective analysis of meteorological fields. In Russian, Gidrometeorologicheskoe Izdatelstvo (GIMIZ), Leningrad. (English translation, Israel Program for Scientific Translations, Jerusalem, 1965, 242 pp.)
- Hasler, A.E., W.E. Shenk and W.C. Skillman, 1977: Wind estimates from cloud motion: Results from Phases I, II and III of an in situ aircraft verification experiment. *J. Appl. Met.* 16, 812-815.
- Kreitzberg, C.W., 1977: Progress and problems in regional numerical weather prediction, Research Paper, Dept. of Physics and Atmospheric Science, Drexel University, Philadelphia, 27 pp.
- MACC Reference Manual, 1978: Two-dimensional interpolation for UNIVAC 1100 series computers, Academic Computer Center, University of Wisconsin, Madison, Wisconsin.
- Mancuso, R.L. and R.M. Endlich, 1973: Wind editing and analysis program-spherical grid (WEAP-1A). Contract Dabc 04-71-C-0013, Stanford Research Institute, Menlo Park, California, 59 pp.
- Perkey, D.F., 1976: A description and preliminary results from a fine-mesh model for forecasting quantitative precipitation, *Mon. Wea. Rev.*, 104, 1513-1526.
- _____, D.F., 1977: Sensitivity of squall-line precipitation an initial low-level humidity. Preprint Volume, Sixth Conference on Weather Forecasting and Analysis, May 10-13, 1976, Albany, New York, 166-173.
- Suchman, D. and D. Martin, 1976: Wind sets from SMS images: An assessment of quality for GATE. *J. Appl. Met.*, 15, 1265-1278.
- Wilson, T.A. and D.D. Houghton, 1979: Mesoscale wind fields for a severe storm situation determined from SMS cloud observations. *Mon. Wea. Rev.*, 107 (to appear in September issue).